The Cryosphere Discuss., 5, 2061–2114, 2011
www.the-cryosphere-discuss.net/5/2061/2011/
doi:10.5194/tcd-5-2061-2011

The Cryosphere Discussions

Spatial and temporal variability of snow accumulation in Dronning Maud Land, East Antarctica, including two deep ice coring sites at Dome Fuji and EPICA DML

S. Fujita[1], P. Holmlund[2], I. Andersson[3], I. Brown[2], H. Enomoto[4,1], Y. Fujii[1], K. Fujita[5], K. Fukui[1,*], T. Furukawa[1], M. Hansson[2], K. Hara[6], Y. Hoshina[5], M. Igarashi[1], Y. Iizuka[7], S. Imura[1], S. Ingvander[2], T. Karlin[2], H. Motoyama[1], F. Nakazawa[1], H. Oerter[8], L. E. Sjöberg[3], S. Sugiyama[7], S. Surdyk[1], J. Ström[9], R. Uemura[10], and F. Wilhelms[8]

[1]National Institute of Polar Research, Research Organization of Information and Systems, Tokyo, Japan
[2]Department of Physical Geography and Quaternary Geology, Stockholm University, Stockholm, Sweden
[3]Division of Geodesy and Geoinformatics, The Royal Inst. of Tecknology, Stockholm, Sweden
[4]Kitami Institute of Technology, Kitami, Japan

[5]Graduate School of Environmental Studies, Nagoya University, Nagoya, Japan
[6]Department of Earth System Science, Faculty of Science, Fukuoka University, Fukuoka, Japan
[7]Institute of Low Temperature Science, Hokkaido University, Sapporo, Japan
[8]Alfred Wegener Institute for Polar and Marine Research, P.O. Box 120161, 27515, Bremerhaven, Germany
[9]Department of Applied Environmental Science, Stockholm University, Stockholm, Sweden
[10]Faculty of Science, Department of Chemistry, Biology, and Marine Science, University of the Ryukyus, Okinawa, Japan
[*]now at: Tateyama Caldera Sabo Museum, Toyama, Japan

Received: 10 July 2011 – Accepted: 29 July 2011 – Published: 8 August 2011

Correspondence to: S. Fujita (sfujita@nipr.ac.jp)

Published by Copernicus Publications on behalf of the European Geosciences Union.

Abstract

To better understand the spatio-temporal variability of the glaciological environment in Dronning Maud Land (DML), East Antarctica, investigations were carried out along the 2800-km-long Japanese-Swedish IPY 2007/2008 traverse. The route covers ice sheet ridges and two deep ice coring sites at Dome Fuji and EPICA DML. The surface mass balance (SMB) distribution was derived based on analysis of isochrones within snow pits, firn cores and subsurface radar signals. The SMB averaged over various time scales in the Holocene was determined. This was then compared with various glaciological data. We find that the large-scale distribution of the SMB depends on the surface elevation, continentality and interactions between ice sheet ridges and the prevailing counterclockwise windfield in DML. A different SMB is found for the windward and leeward sides of the ridges. Local-scale variability in the SMB is essentially governed by bedrock topography which determines the local surface topography. In the eastern part of DML, the accumulation rate in the second half of the 20th century is found to be higher by 15 % compared to averages over longer periods of 722 a or 7.9 ka before AD 2008. A similar trend has been reported for many inland plateau sites in East Antarctica.

1 Introduction

Sea-level rise has been a debated issue in recent climatological studies related to global warming (Lemke et al., 2007). One of the main uncertainties arises from the still unknown contribution of the Antarctic ice sheet (Alley et al., 2005). Hence, assessing the mass balance and surface mass balance (SMB) of the Antarctic ice sheet has been a major concern of recent studies (Arthern et al., 2006; Chen et al., 2006; Davis et al., 2005; Giovinetto and Zwally, 2000; Helsen et al., 2008; Van de Berg et al., 2006; Velicogna and Wahr, 2006). In addition, several approaches for constraining the mass balance of the Antarctic ice sheet are based on the interpolation of accumulation rates

TCD
5, 2061–2114, 2011

obtained from field data such as firn cores, snow pits or stake readings, sometimes using background fields from satellite data to control the interpolation scheme (Arthern et al., 2006; Giovinetto and Zwally, 2000; Vaughan et al., 1999). However, large parts of the vast East Antarctic Plateau remain uncovered by the ground-based measurements needed for these continent-wide interpolations. In response to the necessity of obtaining thorough data sets from the East Antarctic Plateau, recent traversing investigations (e.g. Anschütz et al., 2009; Müller et al., 2010) have provided reliable data sets based on ground-based accumulation measurements using firn cores in addition to subsurface radar, through large parts of Dronning Maud Land (DML) to the South Pole, covering about 2600 km in total. These studies have shown that the spatial pattern is mainly influenced by elevation and continentality, and that several sites exhibit a decrease of more than 20 % in accumulation for the time period 1815–2007 compared to accumulation rates during the period 1641–1815. This suggests that more data are needed for the largely uncovered area of the East Antarctic interior. It has also been pointed out that an increase in the accumulation rate on the high plateau of DML in the late 20th century, proposed in some earlier studies (Hofstde et al., 2004; Mosley-Thompson et al., 1999) needs to be further investigated.

To better understand the spatial distribution of the Antarctic glaciological environment in terms of climatic change, a 2800-km-long traverse was carried out by the Japanese Swedish Antarctic Expedition (henceforth, JASE traverse) across DML in austral summer 2007/2008. The routes included two major ice coring sites at Dome Fuji and at EPICA DML (see Fig. 1 and Table 1), and major ridges and ridge branches between these two sites. The entire routes covered areas in both the Antarctic Southern Atlantic Ocean sector and the Antarctic Indian Ocean sector, with a longitudinal coverage between ∼13° W and ∼42° E. We carried out thorough investigations on glaciological conditions such as SMB, surface elevation, surface slope, prevailing windfield, ice thickness and normal backscattered strength of VHF radio waves from within the ice. For the SMB investigation, we analyzed the age and water equivalent depth of isochrones within snow pit and firn core samples, and using subsurface radar signals. In addition,

TCD
5, 2061–2114, 2011

we used meteorological observational data from automatic weather stations (AWSs) set at several sites along the JASE traverse. Moreover, we used the polarization ratio of satellite-based microwave emissivity data to clarify the spatial variability of the depositional environment over a wide region of DML. Compilation of the data sets allowed the spatial distribution of the SMB to be determined, in addition to its relation to the depositional environment along the traverse and in the surrounding areas in DML. We discuss the large-scale trends in the SMB over a distance of several hundred kilometres in addition to scales as small as a few kilometres, and its dependence on various glaciological conditions. We also argue that there has been a trend towards higher accumulation rates in the second half of the 20th century and that a similar trend has been reported for many sites on the inland plateau in East Antarctica.

2 Traverse route and methods of investigation

2.1 Traverse route

Figure 1 shows a map of DML with the traverse route indicated. The names of important sites on the map are listed in Table 1. The tracked-vehicle-based expedition used two starting points, the S16 site near the Japanese Syowa Station for the Japanese team and the Swedish Wasa Station for the Swedish team. The JASE traverse was along the trace connecting several Antarctic stations, Syowa-Dome Fuji-EPICA DML (Kohnen)-Wasa. The expedition began on 14 November 2007, for the Japanese team and on 5 December 2007, for the Swedish team, with a plan to meet at the meeting point (MP) on the polar plateau in late December, for joint scientific studies and exchange of crew members and scientific instruments such as radars, microwave radiometers and GPS receivers. Many of these scientific instruments were mounted on the vehicles, and were operated continuously along the traverse route. In addition, a new Argos-type AWS was installed at MP (Keller et al., 2010). The two teams met on 27 December at MP and began the return trip to their home stations, Syowa and Wasa,

TCD
5, 2061–2114, 2011

along routes partially different from the incoming ones (blue traces in Fig. 1) for both scientific and logistical reasons.

The JASE traverse route is in the Shirase Glacier Drainage basin in the leg between S16 and Dome Fuji. We refer to this leg as the Dome Fuji route, and it has been used since 1992 (e.g. Furukawa et al., 1996) for management of deep ice coring at Dome Fuji. In the leg between Dome Fuji and A28 (Fig. 1), the traverse is along the main ridge of the ice sheet. In the leg between the A28 site and EPICA DML, the traverse route is located along one of three ridge branches originating from A28. For convenience, in the present paper, we label the ridges DML-A to DML-E, as shown in Fig. 1. Among the three ridge branches labelled as DML-A, DML-B, and DML-C, DML-A is located at the southernmost, interior side of the Antarctic continent. Along the main ridge, the prevailing wind direction is between NE and ENE, as we will discuss later in this paper. Thus, the NNE and SSW sides of the main ridge always represent the upwind and leeward sides, respectively, which influences the accumulation environment. For convenience, we refer to the route between Dome Fuji and the A28 site along the ridge as the "main ridge route" in this paper. We refer to the blue trace in Fig. 1 as the "south route", which represents a depositional environment in contrast to that of the main ridge. The south route is located in the area between the main ridge and the Norway-US traverse 2007/2008 (green dashed trace in Fig. 1). Figure 2 shows a cross section of the ice sheet along the main ridge route and the south route, which gives a large-scale view of surface and bedrock elevation along the traverses.

In addition to these long traverses, we created a survey route orthogonal to the ridge from a point 60 km NNE of MP to a point 20 km SSW of MP. This was carried out to obtain information on the environmental gradient across the ridge. In the present paper, we present data for a 40-km long section of this "cross-ridge" survey centred on MP (orange trace in Fig. 1).

TCD
5, 2061–2114, 2011

2.2 Methods of investigation of accumulation rate

Accumulation rate measurements were carried out using several ground-based methods such as snow pit studies, firn core studies and analysis of isochronous events in subsurface radar signals. This combination of methods, with supporting information from the two deep ice coring sites, provided datasets of the accumulation rate along the traverse averaged over various time scales. We note that a review by Eisen et al. (2008) provided an overview of the various measurement techniques of SMB, related difficulties and limitation of data interpretation.

2.2.1 Snow pit studies

Two 4-m deep pits were dug at a site near Dome Fuji and at MP. In addition, a 2-m deep pit was dug at the DK190 site (Fig. 1 and Table 1). The location of the pit site near Dome Fuji was at 77.298° S and 39.786° E, about 3 km from the station in the northeast direction, and was upwind of the prevailing wind to avoid possible chemical contamination from the station. Chemical constituents were analyzed with a depth resolution of 2 cm at the National Institute of Polar Research, Japan. By analysis of the major ions such as non-sea-salt sulphate (henceforth, nss-sulphate), we identified nss-sulphate peaks originating from the Agung (Indonesia) 1963 eruption (Legrand, 1997; Pruett et al., 2004) and/or the Pinatubo (Philippines) 1991 eruption (Jäger et al., 1995; Legrand and Wagenbach, 1999; Trepte et al., 1993) in order to estimate the averaged accumulation rates since deposition of related aerosols in Antarctica. The former Agung eruption occurred in March 1963, and subsequent deposition of nss-sulphate began following a 6 month time lag in Antarctica (Legrand, 1997; Göktas et al., 2002; Pruett et al., 2004; Traufetter et al., 2004). Thus, we use the nss-sulphate peak for the Agung 1963 eruption as a time marker for the year 1964. Similarly, the deposit associated with the Pinatubo 1991 eruption is used as a time marker for the year 1993. Tritium peaks and physical stratification were also used to determine the depth/age relation. Snow density was measured from the wall of the pit with a depth resolution of

TCD
5, 2061–2114, 2011

3 cm, which gave an estimate of the water equivalent depth. Water equivalent depths for the nss-sulphate peaks were divided by the age of the peaks to derive accumulation rates averaged over 44 yr (1964–2007/2008) for the Agung 1963 eruption and averaged over 15 yr (1993–2007/2008) for the Pinatubo 1991 eruption. We estimated that the major source of errors was spatially inhomogeneous deposition (e.g. Kameda et al., 2008), which can affect the depth determination of a target layer as thick as one year's deposition. Naturally, errors for averages over 44 yr for the Agung 1963 eruption are much smaller than those for averages over 15 yr for the Pinatubo 1991 eruption.

2.2.2 Firn core studies

Firn cores with lengths of ~10 m were sampled at the MP, A35 and A28 sites during the 2007/2008 season by the JASE traverse team (Figs. 1 and 2, and Table 1). In addition, data from 14-m-deep firn cores sampled at FB0603, FB0601 and EPICA DML (Figs. 1 and 2, and Table 1) in the 2004/2005 and 2005/2006 seasons by the Alfred Wegener Institute (AWI), Germany, were used in this study. For these firn cores, the dielectric profiling measurements (DEP) (Moore et al., 1989; Wilhelms et al., 1998) were carried out at the AWI to derive depth profiles of the high-frequency-limit electrical conductivity and density with a depth resolution of 5 mm. For all 6 firn cores, the depth corresponding to the Agung 1963 eruption was determined from the electrical conductivity peak that is known to be correlated with the nss-sulphate concentration (e.g. Wilhelms et al., 2005; Wolff , 2000). For some cores, the deeper signal associated with the Krakatau 1883/1884 eruption was used as a reference. For these firn cores, the Pinatubo 1991 signal was not used because the firn cores were very brittle in the shallowest few meters, which made it difficult for them to maintain their shape for the DEP measurements. The accumulation rate was determined in a similar way to that in the pit studies. Water equivalent depths were first derived using the firn core density. These were then divided by the age of the sulphuric acid deposit produced following the eruption. Error estimation was carried out in the same manner as in the pit studies.

TCD
5, 2061–2114, 2011

2.2.3 Analysis of isochronous events by ground penetrating radar

A commercial ground penetrating radar (GPR) system was used to survey the depth of an internal layer that can be interpreted as an isochrone, that is, a constant time horizon. The GPR was a Geophysical Survey Systems Inc. model SIR-3000 with a 270-MHz antenna. This radar was mounted on one of the Japanese tracked vehicles, and used along the traverse routes between the S16 and MP sites. Between Dome Fuji and the MP site, both the main ridge route and the south route were investigated. The antenna was suspended on the side of the tracked vehicle so that it was always around 20 cm above the snow surface. In this study, we analyzed a horizon dated as 1286 AD. It was selected from many other isochronous features for preliminary analysis. It was chosen because it was among the shallowest layers that were traceable over long distances along the traverse for our experimental settings. However, further analysis using a large number of isochrones with different dates should be carried out in the future. The analytical procedure was as follows. First, a data set for the two-way travel time (TWT) of the electromagnetic waves was compiled along the traverse (Fig. 3). TWT to depth conversion was carried out using the depth-density relation determined at the Dome Fuji coring site (Watanabe et al., 1997). The wave velocity along the propagation path was determined using the empirical relation between density and wave velocity (Fujita et al., 2000; Kovacs et al., 1995). This procedure enabled us to determine the depth of an observed internal layer at the Dome Fuji coring site. The corresponding age of the layer was then assigned based on dating of firn cores at Dome Fuji (Igarashi et al., 2011). Water equivalent depths for the layers were determined assuming the same density profile as that measured for the Dome Fuji ice core, which was further cross-checked by the density profile of the Dome Fuji pit obtained in the present study. Finally, the water equivalent depths were divided by the age of the isochrone to derive the annual accumulation rate. In reality, depth-density profiles should have local variations, which must be taken into account during calculation of the accumulation rate. However, we estimated that the error caused by the local variability

TCD
5, 2061–2114, 2011

of the depth-density relations in traces from the plateau near Dome Fuji is a few % at most. This estimation is based on comparison between the water equivalent depth profile at Dome Fuji and EPICA DML (Ruth et al., 2007). The difference was found to be only ∼6 % at most despite a difference in elevation of ∼900 m. In addition, the 3 pits in the JASE traverse and surface snow measurements (Fujita et al., 2008) showed little local variability.

2.2.4 Analyses of isochronous events in snow radar data

For the legs between Wasa station and MP, a step frequency radar that detects conditions at shallow (<∼70 m) depths (Hamran and Aarholt, 1993; Hamran et al., 1995; Richardson et al., 1997) was used. This radar is referred to as a "snow radar". Again, isochronous features were first detected, and then traced over long distances along the traverse. As was the case for GPR, for preliminary analysis, we selected a single layer from the many traceable layers at each location.

The analytical procedure was as follows. A prominent internal layer at a depth of 7.09 m at MP was first selected for the preliminary analysis. The average snow density from the MP firn core to this depth (∼450 kg m^{-3}) was used to calculate the depth of the layer based on a wave propagation speed of $\sim 2.35 \times 10^8$ m s^{-1}. The layer was tentatively dated to 79.3 yr old by scaling (in water equivalent depth) the Agung 1963 eruption signal (45 yr old) found at 4.6 m depth in the firn core to a depth of 7.09 m. This scaling procedure implies that the estimated accumulation rate can be discussed only within this constraint. That is, we cannot compare values of the accumulation rate before and after the Agung 1963 eruption. This 79.3 yr old layer was traced to a point longitude of 7.00° E which is close to the A23 site (Fig. 1 and Table 1). In the leg with a longitudinal coverage between 7.00° E and 2.10° E, the same 79.3 yr old layer was not traceable. Instead, a deeper layer dated tentatively to 95.5 yr was traced. Also, in the leg with a longitudinal coverage between 2.10° E and 0°, a shallower layer dated tentatively to 57 yr was traced. Dating for these layers was achieved by linear scaling of the first isochrone of the 79.3 yr old at MP. However, because of the date scaling at MP,

TCD
5, 2061–2114, 2011

detailed discussion of the absolute values of accumulation rate is not possible. Instead, we use the accumulation rate values of the firn cores and an earlier compilation of accumulation rate data (Rotschky et al., 2007) in the same DML region as a reliable reference. We adjusted the values of the accumulation rate to these references. In this way, we use the snow radar data only for discussion of variability and not temporal changes in the values.

2.2.5 Analysis of isochronous events in deep radar sounder data

To observe deeper into the interior of the ice sheet, three radar sounders were used. These were (i) a 179-MHz pulse-modulated radar which detects phase and polarization both along and across the track (henceforth, POL179 radar), (ii) a 179-MHz pulse-modulated radar (Fujita et al., 1999; Matsuoka et al., 2002) (henceforth, VHF179 radar) and (iii) a 60-MHz pulse modulated radar (Fujita et al., 1999; Matsuoka et al., 2002) (henceforth, VHF60 radar). All three radars had a peak power of 1 kW and three-element Yagi antennae. With the POL179 radar, a 60-ns pulse was used to detect internal layers. To measure the thickness of the ice sheet, the pulse 500 ns or 1000 ns was used for the three radars. These radars were operated continuously along the traverse route. The POL179 radar was used in the legs between S16 and MP, including both the main ridge route and the south route (see Fig. 1) to measure ice thickness and to observe internal layers. The VHF179 radar was used in the legs between Wasa and MP to measure ice thickness. The VHF60 radar was used between EPICA DML and Dome Fuji to measure ice thickness.

Prominent and persistent internal layers were traced from the raw data of the POL179 radar along the legs near Dome Fuji. From the many internal layers present, we used a layer dated at 7.9 ± 0.5 kyr BP, based on the Dome Fuji ice core, for analysis of the accumulation rate. This layer is deeper than ~200 m, but it is the shallowest prominent and persistent internal layer that was traceable at most of sites including Dome Fuji. For the pulse-modulated radar, the receiver was switched off during pulse transmission in order to protect it from direct transmission. The depth of this layer

TCD
5, 2061–2114, 2011

was 242 m at Dome Fuji and 319 m at MP. Though there were many older and deeper prominent internal layers, we analyzed only this shallow layer because the effect of vertical strain is more difficult to take into account in deeper parts of the ice sheet. The 7.9 ± 0.5 kyr BP layer is located at depths shallower than 10 % of the water equivalent total thickness. Thus, the effect of strain is just a few percent when determining the accumulation rates from the water equivalent depths of the layer.

The analytical procedure used was similar to that for the other radar data. First, a data set for the TWT of the electromagnetic waves was created along the traverse. The depth of the internal layer was accurately determined using a set of calibration data from a down-hole radar target experiment at Dome Fuji (S. Fujita et al., unpublished data, 1997). We used the TWT for a radar target (ice coring drill) placed at accurately known depths in the ice coring hole. In order to calibrate the TWT data, we used electrical conductivity profile data from the Dome Fuji Station ice core (Fujita et al., 2002a) to identify the depths of major reflection boundaries within the ice sheet. The calibrated TWT allowed us to accurately identify the depths of the reflecting boundaries. The age of the layer was then determined using existing dating data for the Dome Fuji ice core (Parrenin et al., 2007). By dividing the water equivalent depth by the age and correcting for vertical strain, the average annual accumulation rate was determined. To correct for the effect of vertical strain on the water equivalent thickness, we used a thinning function based on a 1-D ice flow model at Dome Fuji (Parrenin et al., 2007) instead of a 3-D ice flow model (e.g. Huybrechts et al., 2009). The former model was designed specifically for ice coring sites such as Dome Fuji and Dome C, and has the advantage of being highly tuneable using information from ice cores. Ruth et al. (2007) showed that a 1-D glaciological ice flow model cannot be employed to determine a realistic chronology at EPICA DML coring site for an ice time scale of up to 10^5 yr, because of the complex history of ice flow and accumulation rate along the flow path upstream of EPICA DML. In the present case, our analysis is limited to the summit region between MD550 and MP (Figs. 1 and 2) and to the shallow 7.9 kyr BP layer. Because the horizontal ice flow velocity is very small (<1 m s^{-1}) (e.g. Motoyama et al.,

TCD
5, 2061–2114, 2011

1995; Huybrechts et al., 2009), we assume that a 1-D glaciological ice flow model is still practical so long as we are willing to accept a small amount of error. For example, the ratios of the water equivalent depth for the 7.9 kyr BP layer to the entire thickness at Dome Fuji and MP were 6.4 % and 9.3 %, respectively. Considering the effect of vertical compression (Fig. 5 in Parrenin et al., 2007), we applied a 3.5 % correction for the entire leg to account for vertical strain. We estimate that the error related to this thinning correction is at most ±1.0 %. Later in this paper, we will readdress the point of how the choice of flow model caused differences in the analyzed results.

2.3 Methods of investigation of the prevailing windfield

The prevailing windfield along the JASE traverse routes was investigated in two ways. Strong and persistent winds over the Antarctic ice sheet engrave the snow surface resulting in various types of reliefs, whose orientations can be used as proxy data for the prevailing wind directions. Sastrugi are classified as erosional structures with sharp ridges. Large dunes with heights of more than about 20 ~ 30 cm and with smooth surfaces are depositional structures produced by very strong winds in the presence of snowfall. For both of these structures, the long axis indicates the wind direction. Earlier data for Eastern Dronning Maud Land and Enderby Land were compiled as a folio by Kikuchi (1997). Birnbaum et al. (2010) investigated strong-wind events and their influence on the formation of snow dunes at EPICA DML. They reported that the formation of snow dunes only occurred for high wind speeds of $>10\,\mathrm{m\,s^{-1}}$ at a height of 2 m caused by the influence of a low-pressure system. In this study, the orientation of the surface reliefs was measured using GPS compasses and/or magnetic compasses. The measurements were typically carried out every 10 km. To maintain homogeneous data quality, the same observer performed the measurements over as long a distance as possible. For the 1800-km-long leg from Dome Fuji to Wasa through EPICA DML along the main ridge, only H. Enomoto acted as an observer. For the 900-km-long leg used for the Japanese teams' return trip from MP to MD364 through Dome Fuji, only S. Fujita acted as an observer.

TCD
5, 2061–2114, 2011

The prevailing windfield was further analyzed using meteorological data recorded by an AWS installed by the JASE traverse team at MP. This is the only AWS providing data for the inland plateau of DML between Dome Fuji and EPICA DML. The AWS was prepared by the Antarctic Meteorological Research Center and Automatic Weather Stations Project, Space Science and Engineering Center, University of Wisconsin, Madison. The station name "JASE2007" was allocated to MP (Keller et al., 2010). The JASE2007 AWS has been operational since January 2008, and the data are available online (http://amrc.ssec.wisc.edu/). The observational items are temperature, air pressure, wind speed and wind direction. From these, we used wind speed and wind direction to investigate the relation between them. In addition, earlier AWS data at Dome Fuji (Takahashi et al., 2004), at MD364 (Takahashi et al., 2004) and at EPICA DML (Birnbaum et al., 2010; Reijmer and Van den Broeke, 2003) were also used to investigate the relation between wind speed and direction.

3 Results

3.1 Snow pit and firn core data

Annual accumulation rates averaged over periods after the Agung 1963 eruption and the Pinatubo 1991 eruption are listed in Table 2. They are also displayed as symbols in Figs. 4a and 5a, which show data along the main route and the south route, respectively. We note that the accumulation rate is lower when the elevation is higher along the ridge. The point at FB0603 shows a somewhat lower value than surrounding data points from the firn core studies.

3.2 GPR and snow radar data

Figure 3 shows the TWT and depth of one of the prominent layers along the ridge and the southern route. Several features can be identified in this figure: (i) generally, the

TCD
5, 2061–2114, 2011

Dome Fuji area shows low values; (ii) along the main ridge route, the TWT values are smoother and larger than for the south route; (iii) there are large fluctuations of up to ~20 % along the south route and along the Dome Fuji route close to MD550; (iv) values are generally lower along the south route than along the main ridge route. Using the procedure described in Sect. 2.2.3, the annual accumulation rate averaged over 722 yr (1286–2008) was determined, and the results are shown in Figs. 4a and 5a as blue traces.

The accumulation rates determined by the snow radar are shown as green traces in Figs. 4a and 5a. As described in Sect. 2.2.4, averaging was performed over a variable time span of 57–95.5 yr. At the MP site, the snow radar result is identical to the accumulation rate since the Agung 1963 eruption because the Agung 1963 layer was used as a scaling reference for the dating procedure.

3.3 Deep radar sounding data

Figure 2a and b show the 7.9 ka BP layer and the elevation of the bed in the cross section of the ice sheet. Despite the large variation of ice thickness from ~2500 to ~3400 m in the plateau region, layering of the 7.9 ka BP layer is much smoother than the bedrock elevation. Based on the procedures described in Sect. 2.2.5, the accumulation rates averaged over 7.9 ka were determined and are plotted in Figs. 4a and 5a. We find that the values and variability of the 7.9 ka average are very similar to those of the 722 a average, despite a difference in age span of more than 10 times.

3.4 Prevailing windfield

Figure 6 shows the dominant orientation of surface snow reliefs, such as sastrugis and dunes, observed along the traverse routes between MD364 and Wasa. The orientations are plotted as thin short lines with different colours on the map. At some sites, two or more orientations were observed, in particular at sites between A28 and A23 along the ridge DML-A. In the field, the most dominant orientation was determined first, with secondary or less dominant orientations recorded when necessary.

TCD
5, 2061–2114, 2011

Figure 7a shows meteorological data from the JASE2007 AWS at MP in the year 2009. Wind speed is plotted versus wind direction at intervals of three hours. Wind speeds above 10 m s^{-1} were only observed in 6 % of cases, with an average wind direction of 70 ± 24°. Wind speeds between 5 and 10 m s^{-1} were observed in 36 % of cases, with an average wind direction of 76 ± 35°. About 58 % of wind speeds were less than 5 m s^{-1} with an average wind direction of 97 ± 58°. Average direction of wind vector was also calculated from the meteorological data. It was 82° as indicated as one of yellow arrows in Fig. 6. Near MP, the dominant orientation of surface snow reliefs (Fig. 6) was 70 ± 10°, which is in agreement with the wind direction for strong wind events (>10 m s^{-1}).

In addition to the meteorological data recorded at MP, we examined meteorological data from Dome Fuji, MD364 and EPICA DML sites using the data source described in Sect. 2.3. Figure 7b shows data from the CMOS-type AWS at Dome Fuji in a period between 1994 and 2001. Figure 7c shows data from the Argos-type AWS at MD364 in a period between 2001 and 2003. Table 3 shows a comparison between the dominant orientations of surface snow reliefs and the analyzed wind directions. Orientations of surface snow reliefs tend to agree with wind directions for strong-wind events, rather than average direction of wind vector.

4 Discussion

4.1 Interpretation of snow surface engraving by windfield

We discuss the prevailing windfield first because it influences much of the discussion concerning the spatial distribution of the depositional environment. In particular, the windfield has a direct impact on the flow of maritime air masses over DML and the redistribution of snow deposits. Based on the dominant orientation of surface snow reliefs, we could deduce the direction of the windfield that engraved the snow surface, and this is shown as thick black arrows in Fig. 6. They have an easterly component as

TCD
5, 2061–2114, 2011

was shown in an earlier compilation of snow surface relief data (Kikuchi, 1997) and by mathematical modelling of the prevailing windfield (e.g. Kikuchi and Ageta, 1989; Van den Broeke and Van Lipzig, 2003; Van Lipzig et al., 2004). Along the route between A28 and A23, snow reliefs with multiple different orientations suggest that the wind in this area is more variable than in other areas. Since all of the observations in this area were performed by the same individual, fluctuations in the data quality are unlikely to be a factor here.

A question arises as to how the dominant orientations of the surface snow reliefs represent the windfield. At MP, Dome Fuji and EPICA DML, the directions of strong-wind events agree well with the dominant orientation of the surface snow reliefs, and tend to be rotated counterclockwise with respect to the average wind vectors that are indicated as yellow arrows in Fig. 6. At MD364, the observed orientation of surface snow features was ∼102° and is within variable range of the wind direction for strong-wind events, 120°± 22° (see Table 3). The fact that common features exist in both the western and eastern sides of DML suggests that there are common conditions that cause strong-wind events.

Kikuchi (1997) reported that the orientations of sastrugi, averaged over time and space, agree fairly well with the winter wind direction at Mizuho and near Dome Fuji. In the present study, at MP, time-series data for wind speeds during the year 2009 (not shown) suggested that in winter and spring from May to October, strong winds occur more frequently than during the rest of the year. Kameda et al. (2008) has shown that at Dome Fuji the standard deviation (SD) of the monthly mean SMB was significantly correlated with the monthly mean wind speed, using data from 36 snow stakes observed over 4 yr. They found that a larger SD and monthly mean wind speed occurred in winter. Birnbaum et al. (2010) discussed the characteristics of strong-wind and dune-formation events at EPICA DML. They found that strong-wind events occur more frequently in winter and spring than in summer and fall, forming barchan-type dunes. Thus, these reports are in agreement that strong-wind events occur more frequently in winter and that snow surface reliefs are formed by such events.

TCD
5, 2061–2114, 2011

Watanabe (1978) identified two different wind systems using data for 1977 at Mizuho Plateau in DML: one is almost always directed approximately 60–90° counterclockwise from the downslope direction, while the other has a larger counterclockwise tilt, even pointing upslope in the dome area of high latitudes. Watanabe (1978) suggested that the former represents the katabatic wind which prevails over the gently sloping ($2 \sim 3 \times 10^{-3}$) plateau area, while the other is caused by blizzards, which are severe snowstorms characterized by strong winds. In addition, Kikuchi (1997) found that the prevailing windfields during blizzards had upslope components and were widely observed in an area between 30° E and 50° E in DML. Birnbaum et al. (2010) found that all strong-wind and, hence, all barchan-type dune formation events at EPICA DML identified in a 7 yr period were caused by the influence of a low-pressure system. They also found that in the majority of strong-wind and dune formation events, the near-surface wind turned counterclockwise, indicating cyclonic activity as the main cause for unusually high wind speeds at EPICA DML. Birnbaum et al. (2010) further suggested that enhanced katabatic flow is not the reason for the unusually high near-surface wind speeds at EPICA DML, which is in accordance with the findings by Van As et al. (2007) that the largest near-surface wind speeds at EPICA DML are caused by strong large-scale forcing.

Based on data obtained in the present work and earlier studies, we suggest common conditions throughout DML as follows. In the inland plateau of DML, between MD364 and EPICA DML, strong-wind events engrave the surface snow, forming sastrugis and dunes and redistributing the snow. Cyclonic activity due to low-pressure systems turns the windfield counterclockwise relative to the katabatic wind. Such turns were clearly found at least at three sites along the ridges, Dome Fuji, MP and EPICA DML. As a result, strong winds with upslope components occur throughout DML. In addition, strong-wind events direct maritime air masses over DML. Such events occur more frequently in winter and spring than in summer and fall (Birnbaum et al., 2010). These overall conditions should be considered when attempting to understand the distribution of the accumulation environment at different spatial scales in DML, as discussed below.

TCD
5, 2061–2114, 2011

4.2 Cross-check of the accumulation rate data at Dome Fuji

We next compare the accumulation rate data from the present study with data presented in earlier publications for the purpose of cross-checking. The full set of data used for comparison is listed in Table 2. At Dome Fuji, using 36 bamboo stakes, Kameda et al. (2008) estimated the mean accumulation rate over the period from 1995 to 2006 as $27.3 \pm 0.4\,\mathrm{kg\,m^{-2}\,a^{-1}}$. Figure 8 in Kameda et al. (2008) shows this error which is the standard error of the mean annual SMB for multi-year averages. This result is also plotted in Figs. 4a and 5a, and is close to the average accumulation rates after 1964 AD (the Agung 1963 eruption). Igarashi et al. (2011) estimated the average from AD 1260 to 2001 to be $25.5\,\mathrm{kg\,m^{-2}\,a^{-1}}$ based on the measured concentration of nss-sulphate in a Dome Fuji shallow ice core from the surface to a depth of 40 m. Their estimation agrees well with the average value of $25.1 \pm 0.5\,\mathrm{kg\,m^{-2}\,a^{-1}}$ over 722 a (1286–2008) obtained from GPR measurements. We should note that our dating scale for the GPR data is based on Igarashi et al. (2011). Thus, the agreement should be natural. Nevertheless, the water equivalent depth is determined independently in the GPR work in the present study and the ice core work by Igarashi et al. (2011). Igarashi et al. (2011) further estimated that the average accumulation rates from AD 1888 to 1993, and from AD 1993 to 2001 were 28.3 ± 0.4 and $29.5 \pm 5.2\,\mathrm{kg\,m^{-2}\,a^{-1}}$, respectively. These values are close to those obtained in the present study, the average accumulation rates after 1964 AD (the Agung 1963 eruption), after 1993 (the Pinatubo 1991 eruption), and the value for 1995–2006 from the bamboo stake measurements (Kameda et al., 2008). In this way, the new data from the JASE traverse are consistent with earlier studies at Dome Fuji on different time scales.

TCD
5, 2061–2114, 2011

4.3 Spatial distribution of SMB

4.3.1 Large-scale trend based on ground-based data

The observed accumulation rate is basically dependent on the elevation, continentality and geographical location of the sites relative to the location of the ice sheet ridge and the prevailing windfield in DML, which we will now demonstrate using data. The elevation dependency is shown in Fig. 8 both for the main ridge route (Fig. 4) and for the south route (Fig. 5). From Figs. 4, 5 and 8, we observe that the accumulation rate is lower at higher elevation. Another important trend is that the accumulation rate is lower for the south route than for the main ridge route. This situation can be understood by comparing Figs. 4a and 5a. Also, in Fig. 8a, the data along the main ridge and along the south route are clearly distributed at different levels. In addition, the data along the main ridge is stable and smooth (Figs. 4a and 8a) whereas that along the south route is subject to large fluctuations (Figs. 5a and 8a). Another large-scale trend is that along the ridge branch between the A28 site and EPICA DML, the accumulation rate is fluctuating. Such a pattern is also visible on the accumulation map compiled by Rotschky et al. (2004, 2007). We also note that in the leg between A28 and A23, the accumulation rate is lower than that obtained by a linear interpolation between the accumulation rates on the main ridge route and near EPICA DML (see Figs. 4a and 8a).

The gradient of the accumulation rate versus distance along the main ridge is −0.02 ($kg\,m^{-2}\,a^{-1}$)$\,km^{-1}$ (negative toward higher elevation) for the leg between Dome Fuji and MP in Fig. 4a. Also, the gradient of the accumulation rate versus elevation along the main ridge is −0.04 ($kg\,m^{-2}\,a^{-1}$)$\,m^{-1}$ (negative toward higher elevation). To better understand the gradient of accumulation rate across the ridge, data from the cross-ridge survey at MP was analyzed. The accumulation rate along a 40-km leg is shown in Fig. 9a, together with information on surface elevation, surface slope and bed elevation (Fig. 9b, c and e, respectively). The accumulation rate data were again derived from the GPR and POL179 radar data that give the 722 a average and the 7.9 ka average, respectively. The gradients across the ridge are steep, −0.30 ($kg\,m^{-2}\,a^{-1}$)$\,km^{-1}$

TCD
5, 2061–2114, 2011

(negative toward the inland part of the ice sheet) for the 722 a average and −0.18 (kg m^{-2} a^{-1}) km^{-1} for the 7.9 ka average. To further clarify these results, a contour map was made using data for the annual accumulation rate averaged over 722 a, for an area between Dome Fuji and MP, including the cross-ridge survey at MP, and this is shown in Fig. 10. Because our purpose was to visualize large-scale trends in the gradient, for most of the traverse routes the original data was smoothed over a 40-km distance to reduce fluctuations. For the 40-km-long cross-ridge traverse at MP, a regression line was used. We can observe that the gradient in the vicinity of MP is much steeper than that in the vicinity of Dome Fuji. We will discuss this in Sect. 4.3.2.

The relatively low accumulation rate in the leg between A28 and A23 (Figs. 4a and 8a) can be interpreted in terms of the geographical location of the sites relative to the location of the ice sheet ridge and the prevailing windfield in DML. In Fig. 6, the prevailing windfield shows a counterclockwise distribution in DML. As we discussed in Sect. 4.1, cyclonic activity due to low-pressure systems causes strong winds with upslope components over a wide area of DML, directing maritime air masses and re-distributing surface snow. With such a windfield, the ridge branch DML-A is located in the leeward side of the ridge around A28. It is plausible that the ridge causes a rain shadow on the leeward side for the flow of maritime air masses. The upslope wind in the ridge area causes most of the moisture to be released on the windward side of the ridge and subsequent adiabatic warming of dry air can occur within the downslope wind in the leeward area. In addition, the two ridge branches DML-B and DML-C can act as barriers to the movement of maritime moisture into the interior of the continent. It seems likely that the snow reliefs with multiple orientations along this leg are caused by the complex windfield in the lee of these ridge branches.

4.3.2 Large-scale trend inferred from passive microwave data

To further clarify the large-scale trend of the accumulation rate, data from the passive microwave measurements are useful. Previous studies have shown that polarization of the microwave brightness temperature is linked to snow layering (Surdyk and Fily,

TCD
5, 2061–2114, 2011

1993, 1995). The passive microwave data used in this study were obtained from the Advanced Microwave Scanning Radiometer for EOS (AMSR-E), which was developed by JAXA for use on board the EOS satellite and has been in operation since 2002. The AMSR-E sensor measures both vertical and horizontal polarizations at 6.9, 10.65, 18.7, 23.8, 36.5 and 89.0 GHz. For the data used in the present study, the incident angle was approximately 55° from the zenith. The spatial resolution varied from 43 km at 6.9 GHz to 3.5 km at 89.0 GHz. The monthly mean brightness-temperature data for June 2003 were used. The polarization ratio, PR, is defined as follows:

$$PR = \frac{TB_v - TB_h}{TB_v + TB_h}$$

where TB_v and TB_h are the vertical and horizontal components of the brightness temperature. Figure 11 displays the distribution of the polarization ratio at 6.9 GHz, PR6.9. Surdyk and Fily (1993, 1995) found that the PR at frequencies below 10 GHz is a good indicator of the stratification in the snow cover: the higher the PR the larger the number of strata per unit depth, which correlates with a lower accumulation rate. We also note that microwave brightness temperature has little (less than a few kelvin) seasonal variability at frequencies near 6.9 GHz (e.g. Surdyk, 2002). Thus, spatial distribution of the PR6.9 from the monthly mean data for June 2003 represents data for much longer time span.

From Fig. 11, the most important features of the PR6.9 distribution are as follows.

i. The northeast and southwest regions of the map tend to have low and high PR values, respectively. That is, the upwind side of the main ridge tends to have higher accumulation and the leeward side tends to have lower accumulation.

ii. In the area between Dome Fuji and MP, the distribution of the polarization ratio is similar to the distribution of the accumulation rate shown in Fig. 10. For example, there is a gradient observed across the ridge in both cases. The high PR6.9 to the south of Dome Fuji is consistent with the low accumulation rate and the low

TCD
5, 2061–2114, 2011

PR6.9 to the north of MP is consistent with the high accumulation rate. These common features suggest that PR6.9 is well correlated with the distribution of the accumulation rate, at least qualitatively.

iii. The leg between A28 and EPICA DML and the northwest side of A28 are within the high PR6.9 zone, which suggests a low accumulation rate.

iv. There are several ridge branches of the ice sheet in the map. The prevailing windfield is counterclockwise. The upwind side of the ridge branches tend to have lower PR6.9, which suggests a higher accumulation rate. The leeward side of the ridge branches tend to have higher PR6.9, which suggests a lower accumulation rate.

v. The northeast side of MP is located upwind of the ridge branch DML-D connecting MP and Nansenisen near the Sør Rondane Mountains. This explains why a steep gradient in the accumulation rate across the ridge was observed at MP (Figs. 9 and 10). That is, the northern side of MP has a higher accumulation rate because it is upwind of both the main ridge and the ridge branch DML-D to Nansenisen. The southern side of MP is the downwind side.

In summary, the PR6.9 map provides insights into the distribution of the accumulation rate in this area. Qualitatively, the PR6.9 distribution agrees well with our accumulation rate data. Further work should include analysis of the local variability, quantitative analysis, and the development of theoretical models and algorithms to derive the accumulation rate from the polarization ratio data.

4.3.3 Local-scale variability

We next examine the local-scale variability of the depositional environment. In addition to the large-scale trend discussed above, the prevailing wind, local shape of the ice sheet surface and surface slope have a strong influence to the local-scale variability. Therefore, datasets were prepared to assess this influence. The surface slopes

TCD
5, 2061–2114, 2011

were determined using the digital elevation model (DEM) (Bamber et al., 2006) and are shown in Figs. 4b, 5b and 9b. The surface slope is known to strongly influence the spatial distribution of the accumulation rate at various locations on the polar plateau (e.g. the Syowa-South Pole traverse – Endo and Fujiwara, 1973, the Dome Fuji-Syowa route – Fujita et al., 2002b; Furukawa et al., 1996, the DML-South pole traverse – Anschütz et al., 2009; Müller et al., 2010 and near Dome C and Talos Dome – Frezzoti et al., 2005, 2007) because the combination of the prevailing wind, the steepness of the slope and the local surface topography determines the depositional environment. At the local regional scale, we find that there is an anticorrelation between the accumulation rate and the surface slope along the JASE traverse (Figs. 4a, b, 5a, b, 8a, b and 9a, c). This suggests that snow is more easily deposited on a relatively flat surface, particularly if it is somewhat concave (see locations at −12 km and +10 km in Fig. 9a, b for example). We suggest that one of major controlling factors of local variability is the surface slope, as pointed out in the earlier studies mentioned above. In addition, surface slope is highly correlated to bedrock topography, as can be seen from Figs. 4, 5 and 9. Thus, local variations in the accumulation rate are naturally preserved over time. That is, locally high or low accumulation sites tend to remain so over long time scales. In this study, we observed that the spatial variabilities of the 722 a average accumulation rate and the 7.9 ka average accumulation are very similar both along the main ridge (Fig. 4a) and along the south route (Fig. 5a). This is basically due to preservation of the accumulation pattern over these time scales.

Another interesting indicator for the depositional environment is variations in the normal backscatter of VHF radio waves from within the ice, measured using the 179-MHz radar systems. This data is shown in Figs. 4c, 5c and 9d. The values are given only in relative manner in decibel scale. In an earlier study along the Dome Fuji route (Fujita et al., 2002b), the normal backscattering of radio waves at 179 MHz and at 60 MHz was empirically correlated to the surface slope and accumulation rate of the ice sheet. We expect normal backscattering to be stronger from locations where smoother internal layers exist in the ice sheet, considering the basic principles of electromagnetic

TCD
5, 2061–2114, 2011

scattering from slightly rough surfaces (Ulaby et al., 1982). With the POL179 and the VHF179 radars, the shallowest detectable signal is from a depth of ~210 m. This is because the receivers are switched off when the transmission signal is on. At a depth of ~210 m, the primary sources of internal reflection are believed to be stratified fluctuations in density, acidity and/or crystal orientation fabrics (e.g. Fujita et al., 1999), depending on the physical conditions within the ice and the choice of radio frequency. Whatever source is dominant, if the accumulation rate is spatially uniform at the time of deposition, buried strata can give rise to stronger scattering because of higher coherence. It should be noted that we observed radio wave scattering from a single depth and not from an isochronous layer, in order to determine the properties of the scattering surfaces. At a depth of ~210 m the age of the strata is about 5 kyr BP. However, because of preservation of the accumulation pattern over time scales up to 7.9 ka, as discussed above, the scattered power still provides useful information for understanding the present spatial distribution of the depositional environment. Comparing Figs. 4c and 5c, it can be seen that the backscattered power profile is stronger and smoother at the higher elevation near Dome Fuji (Figs. 4 and 5). Also, the Dome Fuji route (Fig. 4) and the coastal side of the ridge (Fig. 9) tend to have larger values of backscattered power. It becomes lower and fluctuates more at positions closer to EPICA DML, particularly along the leg between A38 and EPICA DML. On a local scale, the backscattered power exhibits variations that are sometimes correlated with the surface slope and accumulation rate. Stronger backscattering is seen to occur when the surface slope is less steep and thus the accumulation rate is larger.

4.4 Increase in accumulation rate during the 20th century

Figures 4a, 5a and 8a show a comparison of the annual accumulation rate over different periods of time within the Holocene. We find that in the ~500-km-long leg between Dome Fuji and A35, the average accumulation rates after 1964 AD (the Agung 1963 eruption) and/or after 1993 (the Pinatubo 1991 eruption) are significantly larger than accumulation rates averaged over longer periods (722 a and 7.9 ka). These data suggest

TCD
5, 2061–2114, 2011

an increase in the accumulation rate at least during the second half of the 20th century in the sector between 40° E and 22.5° E.

Such an increase in the accumulation rate can be investigated by reference to several earlier studies in DML. Indeed, ice cores covering a time span of ∼1000 yr have indicated temporal variations of the accumulation rate. Oerter et al. (2000) reported the results of accumulation studies that were conducted during the 1997/98 field season along a 1200-km traverse in Amundsenisen that covers a 10° W–10° W sector of DML. Stacking of 12 annually resolved records, based on pit and shallow firn core studies, produced a composite record of accumulation rates for the last 200 yr. They reported that accumulation rates decreased in the 19th century and increased in the 20th century and concluded that recent values were by no means extraordinary, as they did not exceed those at the beginning of the 19th century. They further concluded that variations in accumulation rates were most probably linked to the temperature variations indicated by δ^{18}O records in Amundsenisen. Hofstde et al. (2004) presented an overview of firn accumulation in DML over the past 1000 yr based on a chronology established with dated volcanogenic horizons in six firn cores. They demonstrated that the mean increase over the early 20th century was the largest within the past 1000 yr. In addition, a study by Igarashi et al. (2011) produced a time series of accumulation rates at Dome Fuji over the last 740 yr, which showed a remarkable resemblance to the data presented by Oerter et al. (2000) and Hofstde et al. (2004) near the EPICA DML site. This suggests that the increase in accumulation rate was widespread in DML during the 20th century. It should be noted that both in Igarashi et al. (2011) and Hofstde et al. (2004), running means of the accumulation rate over the latest 50 yr gave the highest values within the past 740 yr. A compilation of the 37-yr history of net accumulation at the South Pole (Mosley-Thompson et al., 1999) suggested an increase in annual accumulation rate since 1965. These data suggest that the recent increase in accumulation rate extends beyond DML, South Pole region and may be characteristic of the high East Antarctic Plateau. At Dome C, Frezzoti et al. (2005) found a recent accumulation rate increase to 32 $kg^{-2}\,a^{-1}$, which can be compared to a long-term mean

TCD
5, 2061–2114, 2011

of 25.3 kg^{-2} a^{-1} (1815–1998). They also reported a general increase in the accumulation rate at several drill sites along the transect from Terra Nova Bay to Dome C. In their cores, the period 1966–1998 shows a 14 to 55 % higher accumulation rate than the period 1815–1998.

Karlöf et al. (2005) investigated accumulation rates around "site M" (75.0° S, 15.0° E, see Fig. 1) in DML using firn cores and pit studies. They reported that the accumulation rate in the area has been stable over the last 200 yr. Isaksson et al. (1996) observed an accumulation rate decrease over the period 1932–1991 from a coastal core in DML and reported no change in accumulation rate for the period 1865–1991, based on another core from the plateau (75° S, 2° E, 2900 m a.s.l.). In addition, Isaksson et al. (1999) found that a general increase in accumulation rate, particularly in the latter part of the 20th century, was not necessarily the case for the whole polar plateau of DML. These reports disagree with other studies indicating an increase of the accumulation rate in DML. Stenni et al. (2002) found that the accumulation rate at Talos Dome had increased by 11 % during the 20th century in comparison to the 800 yr mean. However, Frezzoti et al. (2007) reported no significant increase in the accumulation rate over the last two centuries near Talos Dome. Yet Urbini et al. (2008) found significantly lower accumulation rates in the southwest of Talos Dome during the period 1835–1920 when compared with the period 1920–2001.

In summary, in the majority of earlier reports and also in the present study, a trend towards increasing accumulation rates during the 20th century is commonly found for the polar plateau, near Dome Fuji, EPICA DML, sites along the ridge between them, the South Pole, Dome C and Talos Dome. However, no significant change was reported for other sites, mainly along the leg between A28 and Troll Station in Fig. 1. The reason for these different results is not immediately clear. However, based on the results of the present study, we suggest two possibilities: (i) no increase in the accumulation rate occurred in the leg between Troll Station (Fig. 1) and site M near the ridge; (ii) these sites are located on the leeward side of ridge branches DML-B and DML-C near the Troll Station with respect to the easterly prevailing wind, which possibly masks any

TCD
5, 2061–2114, 2011

increase in accumulation rate. If this is the case, then it is necessary to carry out further investigations in this area to address questions related to changes in accumulation during the 20th century. We suggest that cross-ridge surveys using ridges DML-B and DML-C would be an effective means of approaching this.

4.5 Comparison with an earlier accumulation rate study along the same ridges

Huybrechts et al. (2009) estimated the accumulation rate along the leg between EPICA DML and Dome Fuji using airborne radar sounding data and 3-D thermomechanical ice sheet modelling. The trace of the survey is shown in Fig. 1 as a yellow dashed line. This flight trace agrees well with the JASE traverse route in the leg between DK190 and A38. In contrast, the two traces tend to deviate by up to ∼10 km at some locations, such as between Dome Fuji and DK190, and between A23 and EPICA DML. In Fig. 4a, the average accumulation rate over 5 ka, from radar sounding and ice sheet modelling (Huybrechts et al., 2009) is compared with the results of the present study. Comparing it with the 722 a average and the 7.9 ka average from the present study, we find differences as large as 10 kg m^{-2} a^{-1}. In addition, the accumulation rate over 5 ka exhibits a larger amount of fluctuation than the accumulation rates for the 722 a average and the 7.9 ka average. The cause of this rather large difference is not immediately clear; it is beyond the scope of this paper to address ice sheet modelling. However, we propose a few possibilities: (i) for some reason, thinning due to vertical strain is overestimated at some locations in the 3-D ice sheet model of Huybrechts et al. (2009); (ii) thinning was underestimated in the present study that used a 1-D ice sheet model at Dome Fuji. It is a clear fact that the present data showed that the 722 a average and the 7.9 ka average had very similar variability both along the main ridge (Fig. 4a) and along the south route (Fig. 5a). Thus, it is highly unlikely that the accumulation pattern changed dramatically between the 722 a average and the 7.9 ka average. The 722 yr isochrone is located at a water equivalent depth of less than ∼1 % of the entire thickness, for which the correction for vertical strain is negligibly small. Thus the 722 a average has virtually no error associated with vertical strain effects. The 7.9 ka average

TCD
5, 2061–2114, 2011

has a very similar profile to the 722 a average, which implies that possibility (i) above is the cause of the observed large difference. We point out that the depths of the internal layers given in Huybrechts et al. (2009) (Fig. 3a in their paper) are very similar to those for the JASE traverse. Therefore, the difference is essentially due to estimation of the vertical strain using ice sheet models.

5 Concluding remarks

In the JASE traverse, we investigated spatial and temporal variability of the ice sheet environment in the sparsely explored inland plateau area of East Antarctica. The major findings of the present study are summarized as follows.

1. In the inland plateau of DML, strong-wind events engrave surface snow, forming sastrugis and dunes and redistributing the snow. Cyclonic activity due to low-pressure systems causes the windfield to rotate counterclockwise relative to the katabatic wind. As a result, strong winds with upslope components are widespread in DML. In addition, strong-wind events direct maritime air masses over DML. Such events occur more frequently in winter and spring than in summer and fall.

2. When strong winds with upslope components blow across the ridges, the air tends to release its moisture on the windward side of the ridge and the leeward side is then exposed to drier air. As a result, a different SMB is found on windward and leeward sides of the ridges.

3. Large-scale variations in the depositional environment depend on surface elevation, continentality and interactions between ice sheet ridges and the counterclockwise prevailing windfield in DML.

4. Local-scale variations in the depositional environment are essentially governed by bedrock topography which determines the local surface topography and the probability of snow deposition.

TCD
5, 2061–2114, 2011

5. In the eastern part of DML from ~15° E to ~40° E longitude, the accumulation rate in the second half of the 20th century is found to be higher by ~15 % compared to averages over longer periods of 722 a and 7.9 ka.

6. This recent increase in accumulation rates is consistent with reports of studies on many sites in the inland plateau of East Antarctica. However, some studies have indicated insignificant increases at sites between Troll Station and site M. We suggest that the geographical location of these sites on the leeward side of the ridge branch near Troll Station with respect to the prevailing easterly wind may lead to any increase in the accumulation rate being masked.

7. The spatial pattern of the accumulation rate was unchanged over the investigated periods along the main ridge route and the south route.

8. In the leg connecting Dome Fuji and EPICA DML, the present ground-based studies that used a 1-D ice sheet model gave a spatial variability in the accumulation rate that was different from that obtained in an earlier study using airborne radar sounding data and a 3-D thermomechanical ice sheet model. It is likely that the 3-D thermomechanical ice sheet model overestimated the strain when processing the raw radar sounding data.

9. A new data set for ice sheet thickness was produced as shown in the figures. This will be used for future international compilation of the ice sheet topography map.

10. A new data set was produced for snow surface reliefs. In addition, meteorological data is available from the JASE2007 AWS at MP.

11. Normal backscattering of electromagnetic waves from the shallow subsurface was shown to be correlated to surface slope, elevation and geographical location in the ice sheet. We suggest that the backscatter is an indicator of the roughness of the buried strata when deposition occurred on the surface.

TCD
5, 2061–2114, 2011

12. The polarization ratio at 6.9 GHz from the passive microwave data is well correlated to the accumulation rate data, at least qualitatively, and provided insights into the large-scale trend of the accumulation rate.

The increase in the accumulation rate in the second half of the 20th century is a topic that should be examined by climatologists in the context of climate change and global warming. In addition, we need to further examine temporal changes of the accumulation rate in East Antarctica. Moreover, we must continue to monitor the surface mass balance in Antarctica to better understand ongoing changes. The present work used several selected time markers in the Holocene. Future analyses should include the use of additional time markers of subsurface radar, firn cores and pit samples to obtain detailed time series information on the accumulation rate. A clearly necessary approach for mass balance studies of the Antarctic ice sheet is to constrain the surface mass balance by interpolation of the accumulation rates obtained from different types of field data, and using background fields from satellite data such as the polarization ratio to control the interpolation scheme. The data obtained in the present study represents a reliable contribution to such an approach. Spatial variability of the accumulation rate is smaller along the ridge than that in regions away from the ridge, suggesting an advantage of using ridge areas for studying temporal variations of the paleoclimatic signals from ice cores.

Acknowledgements. The JASE traverse was organized by several organizations both in Sweden and Japan. The National Institute of Polar Research (NIPR), Tokyo and the Swedish Polar Research Secretariat (SPRS) managed the logistics in Antarctica. Science management was a collaborative effort of NIPR, Stockholm University, the Royal Institute of Technology in Stockholm and individuals from several universities and institutes in Japan. The JASE traverse is one of research projects being undertaken by the Japanese Antarctic Research Expedition "Studies on systems for climate change and ice sheet change, by introducing new observational methods and technologies". This work has been carried out under the umbrella of TASTE-IDEA within the framework of IPY project 152. This work is also a contribution to ITASE. The authors appreciate the support of the Automatic Weather Station Program for the JASE2007 AWS and associated data, NSF grant number ANT-0944018. Thanks are extended to T. Kameda for

TCD
5, 2061–2114, 2011

arrangement of the AWS for the JASE team. AMSR-E data was provided from JAXA/EORC as a part of GCOM-W project. The traverse was fully supported by the teams of the 48th and the 49th Japanese Antarctic Research Expeditions led by H. Miyaoka and S. Imura, respectively. Special thanks go to the logistics members, S. Gunnarsson, H. Kaneko, T. Karlberg, P. Ljusberg and K. Taniguchi and the medical doctors, S. Eriksson and N. Shiga, for their very generous support during the traverse. This research was supported by the Swedish Research Council (VR) and by a Grant-in-Aid for Scientific Research (A) 20241007 from the Japan Society for the Promotion of Science (JSPS).

References

Alley, R., Clark, P., Huybrechts, P., and Joughin, I.: Ice-sheet and sea level changes, Science, 310(5747), 456–460, doi:10.1126/science.1114613, 2005. 2063

Anschütz, H., Müller, K., Isaksson, E., McConnell, J. R., Fischer, H., Miller, H., Albert, M., and Winther, J.-G.: Revisiting sites of the South Pole Queen Maud Land Traverses in East Antarctica: Accumulation data from shallow firn cores, J. Geophys. Res., 114, D24106, doi:10.1029/2009JD012204, 2009. 2064, 2084, 2100, 2104

Arthern, R. J., Winebrenner, D. P., and Vaughan, D.G.: Antarctic snow accumulation mapped using polarization of 4.3-cm wavelength microwave emission, J. Geophys. Res, 111, D06107, doi:10.1029/2004JD005667, 2006. 2063, 2064

Bamber, J. L., Gomez-Dans, J. L., and Griggs, J. A.: Antarctic 1 km Digital Elevation Model (DEM) from Combined ERS-1 Radar and ICESat Laser Satellite Altimetry, in National Snow and Ice Data Center. Digital media, Boulder, Colorado USA, 2009. 2084, 2105, 2107

Birnbaum, G., Freitag, J., Brauner, R., König-Langlo, Schulz, G. E., Schulz, E., Kipfstuhl, S., Oerter, H., Reijmer, C. H., Schlosser, E., Faria, S. H., Ries, H., Loose, B., Herber, A., Duda, M. G., Powers, J. G., Manning, K. W., and Van den Broeke, M. R.: Strong-wind events and their influence on the formation of snow dunes: Observations from Kohnen Station, Dronning Maud Land, Antarctica, J. Glaciol., 56(199), 891–902, doi:10.3189/002214310794457272, 2010. 2073, 2074, 2077, 2078, 2103, 2109

Chen, J., Wilson, C., Blankenship, D., and Tapley, B.: Antarctic mass rates from GRACE, Geophys. Res. Lett., 33, L11502, doi:10.1029/2006GL026369, 2006. 2063

Davis, C., Li, Y., McConnell, J., Frey, M., and Hanna, E.: Snowfall-driven growth in

TCD
5, 2061–2114, 2011

East Antarctic ice sheet mitigates recent sea-level rise, Science, 308, 5730, 1898–1901, doi:10.1126/science.1110662, 2005. 2063

Eisen, O., Frezzotti, M., Genthon, C., Isaksson, E., Magand, O., Van den Broeke, M. R., Dixon, D.A., Ekaykin, A., Holmlund, P., Kameda, T., Karlöf, L., Kaspari, S., Lipenkov, V., Oerter, H., Takahashi, S., and Vaughan, D. G.: Ground-based measurements of spatial and temporal variability of snow accumulation in East Antarctica, Rev. Geophys., 46, RG2001, doi:10.1029/2006RG000218, 2008. 2067

Endo, Y. and Fujiwara, K.: Characteristics of the Snow Cover in East Antarctica Along the Route of the JARE South Pole Traverse and Factors Controlling Such Characteristics, Polar Res. Cent., Natl. Sci. Mus., Tokyo, 38 pp., 1973. 2084

EPICA Community Members: One-to-one coupling of glacial climate variability in Greenland and Antarctica, Nature, 444, 195–198, doi:10.1038/nature05301, 2006. 2100

Frezzotti, M., Pourchet, M., Flora, O., Gandolfi, S., Gay, M., Urbini, S., Vincent, C., Becagli, S., Gragnani, R., Proposito, M., Severi, M., Traversi, R., Udisti, R., and Fily, M.: Spatial and temporal variability of snow accumulation in East Antarctica from traverse data, J. Glaciol., 51, 113–124, doi:10.3189/172756505781829502, 2005. 2084, 2086

Frezzotti, M., Urbini, S., Proposito, M., Scarchilli, C., and Gandolfi, S.: Spatial and temporal variability of surface mass balance near Talos Dome, East Antarctica, J. Geophys. Res., 112, F02032, doi:10.1029/2006JF000638, 2007. 2084, 2087

Fujita, S., Maeno, H., Uratsuka, S., Furukawa, T., Mae, S., Fujii, Y., and Watanabe, O.: Nature of radio-echo layering in the Antarctic ice sheet detected by a two-frequency experiment, J. Geophys. Res., 104(B6), 13013–13024, doi:10.1029/1999JB900034, 1999. 2071, 2085

Fujita, S., Matsuoka, T., Ishida, T., Matsuoka, K., and Mae, S.: A summary of the complex dielectric permittivity of ice in the megahertz range and its applications for radar sounding, in Physics of Ice Core Records, edited by: Hondoh, T., Hokkaido University Press, Sapporo, 185–212, 2000. 2069

Fujita, S., Azuma, N., Motoyama, H., Kameda, T., Narita, H., Fujii, Y., Watanabe, O.: Electrical measurements from the 2503-m Dome F Antarctic ice core, Ann. Glaciol., 35, 313–320, doi:10.3189/172756402781816951, 2002a. 2072

Fujita, S., Maeno, H., Furukawa, T., and Matsuoka, K.: Scattering of VHF radio waves from within the top 700 m of the Antarctic ice sheet and its relation to the depositional environment: a case study along the Syowa-Mizuho-Dome F traverse, Ann. Glaciol., 34, 157–164, doi:10.3189/172756402781817888, 2002b. 2084

TCD
5, 2061–2114, 2011

Fujita, S., Enomoto, H., Kameda, T., Motoyama, H., and Sugiyama, S.: Changes of surface snow density in a summer in the Antarctic Dome Fuji region, paper presented at SCAR/IASC IPY Open Science Conference, Assoc. of Polar Early Career Sci., St. Petersburg, Russia, 8–11 July 2008. 2070

Furukawa, T., Kamiyama, K., and Maeno, H.: Snow surface features along the traverse route from the coast to Dome Fuji Station, Queen Maud Land, Antarctica, Proc. NIPR Symp. Polar Meteorol. Glaciol., 10, 13–24, 1996. 2066, 2084

Giovinetto, M. and Zwally, H.: Spatial distribution of net surface accumulation on the Antarctic ice sheet, Ann. Glaciol., 31, 171–178, doi:10.3189/172756400781820200, 2000. 2063, 2064

Göktas, F., Fischer, H., Oerter, H., Weller, R., Sommer, S., and Miller, H.: A glacio-chemical characterisation of the new EPICA deep-drilling site on Amundsenisen, Dronning Maud Land, Antarctica., Ann. Glaciol., 35, 347–354, doi:10.3189/172756402781816474, 2002. 2067

Hamran, S.-E. and Aarholt, E.: Glacier study using wavenumber domain synthetic aperture radar, Radio Sci., 28(4), 559–570, doi:10.1029/92RS03022, 1993. 2070

Hamran, S.-E., Gjessing, D. T., Hjelmstad, J., and Aarholt, E.: Ground penetrating synthetic pulse radar: Dynamic range and modes of operation, J. Appl. Geophys., 33, 7–14, doi:10.1016/0926-9851(95)90025-X, 1995. 2070

Haran, T., Bohlander, J., Scambos, T., Painter, T., and Fahnestock, M.: MODIS mosaic of Antarctica (MOA) image map, in National Snow and Ice Data Center. Digital media, Boulder, Colorado USA, 2005, updated 2006. 2104

Helsen, M., Van den Broeke, M., Van de Wal, R., Van de Berg, W., Van Meijgaard, E., Davis, C., Li, Y., and Goodwin, I.: Elevation changes in Antarctica mainly determined by accumulation variability, Science, 320, 1626–1629, doi:10.1126/science.1153894, 2008. 2063

Hofstede, C. M., Van de Wal, R. S. W., Kaspers, K. A., Van den Broeke, M. R., Karlöf, L., Winther, J.-G., Isaksson, E., Lappegard, G., Mulvaney, R., Oerter, H., and Wilhelms, F.: Firn accumulation records for the past 1000 years on the basis of dielectric profiling of six cores from Dronning Maud Land, Antarctica, J. Glaciol., 50(169), 279–291, doi:10.3189/172756504781830169, 2004. 2064, 2086, 2100

Huybrechts, P., Rybak, O., Pattyn, F., and Steinhage, D.: Past and present accumulation rate reconstruction along the Dome Fuji-Kohnen radio echo sounding profile, Dronning Maud Land, East Antarctica, Ann. Glaciol., 50(51), 112–120, doi:10.3189/172756409789097513, 2009. 2072, 2073, 2088, 2089, 2104, 2105, 2107

TCD
5, 2061–2114, 2011

Igarashi, M., Nakai, Y., Motizuki, Y., Takahashi, K., Motoyama, H., and Makishima, K.: Dating of the Dome Fuji shallow ice core based on a record of volcanic eruptions from AD 1260 to AD 2001, Polar Sci., in press, 2011. 2069, 2079, 2086, 2101

Isaksson, E., Karlén, W., Gundestrup, N., Mayewski, P., Whitlow, S., and Twickler, M.: A century of accumulation and temperature changes in Dronning Maud Land, Antarctica, J. Geophys. Res., 101(D3), 7085–7094, doi:10.1029/95JD03232, 1996. 2087, 2100

Isaksson, E., Van den Broeke, M. R., Winther, J.-G., Karlöf, L., Pinglot, J. F., and Gundestrup, N.: Accumulation and proxy-temperature variability in Dronning Maud Land, Antarctica, determined from shallow firn cores, Ann. Glaciol., 29(1), 17–22, doi:10.3189/172756499781821445, 1999. 2087

Jäger, H., Uchino, O., Nagai, T., Fujimoto, T., Freudenthaler, V., and Homburg, F.: Ground-based remote sensing of the decay of the Pinatubo eruption cloud at Northern Hemispheric sites, Geophys. Res. Lett., 22, 607–610, doi:10.1029/95GL00054, 1995. 2067

Kameda, T., Motoyama, H., Fujita, S., and Takahashi, S.: Temporal and spatial variability of surface mass balance at Dome Fuji, East Antarctica, by the stake method from 1995 to 2006, J. Glaciol., 54(184), 107–116, doi:10.3189/002214308784409062, 2008. 2068, 2077, 2079, 2101, 2107

Karlöf, L., Isaksson, E., Winther, J.-G., Gundestrup, N., Meijer, H. A. J., Mulvaney, R., Pourchet, M., Hofstede, C.,Lappegard, G., Pettersson, R., Van den Broeke, M., and Van de Wal, R. S. W.: Accumulation variability over a small area in East Dronning Maud Land, Antarctica, as determined from shallow firn cores and snow pits: Some implications for ice-core records, J. Glaciol., 51(174), 343–352, doi:10.3189/172756505781829232, 2005. 2087

Keller, L. M., Lazzara, M. A., Thom, J. E., Weidner, G. A., and Stearns, C. R.: Antarctic Automatic Weather Station Data for the calendar year 2009, Space Science and Engineering Center, University of Wisconsin, Madison, Wisconsin, 2010. 2065, 2074, 2103, 2110

Kikuchi, T.: Prevailing Windfield, in: Antarctica: East Queen Maud Land-Enderby Land Glaciological Folio, Sheet 2, National Institute of Polar Research, Tokyo, Japan, 1997. 2073, 2077, 2078

Kikuchi, T. and Ageta, Y.: A preliminary estimate of inertia effects in a bulk model of katabatic wind, Proc. NIPR Symp. Polar Meteorl. Glaciol., 2, 61–69, 1989. 2077

Koerner, R. M.: A stratigraphic method of determining the snow accumulation rate at Plateau Station, Antarctica, and application to South Pole-Queen Maud Land Traverse 2, 1965–1966, in: Antarctic Ice Studies II, edited by: Crary, A. P., AGU, Washington, D. C., 225–238, 1971.

TCD
5, 2061–2114, 2011

2100
Kovacs, A., Gow, A. J., and Morey, R. M.: The in-situ dielectric constant of polar firn revisited, Cold Reg. Sci. Technol., 23(3), 245–256, doi:10.1016/0165-232X(94)00016-Q, 1995. 2069
Legrand, M.: Ice-core records of atmospheric sulfur, Philos. T. R. Soc. Lon. B, 352(1350), 241–250, doi:10.1098/rstb.1997.0019, 1997. 2067
Legrand, M. and Wagenbach, D.: Impact of Cerro Hudson and Pinatubo volcanic eruptions on the Antarctic air and snow chemistry, J. Geophys. Res., 104(D1), 1581–1596, doi:10.1029/1998JD100032, 1999. 2067
Lemke, P., Ren, J., Alley, R. B., Allison, I., Carrasco, J., Flato, G., Fujii, Y., Kaser, G., Mote, P., Thomas, R. H., and Zhang, T.: Observations: Changes in Snow, Ice and Frozen Ground, in: Climate change 2007: the physical science basis. Contribution of Working Group I to the Fourth Assessment Report of the Intergovernmental Panel on Climate Change, edited by: Solomon, S., Qin, D., Manning, M., Chen, Z., Marquis, M., Averyt, K. B., Tignor, M., and Miller, H. L., Cambridge University Press, Cambridge, 2007. 2063
Müller, K., Sinisalo, A., Anschütz, H., Hamran, S.-E., Hagen, J.-O., McConnell, J. R., and Pasteris, D. R.: An 860 km surface mass-balance profile on the East Antarctic plateau derived by GPR, Ann. Glaciol., 51(55), 1–8, doi:10.3189/172756410791392718, 2010. 2064, 2084, 2100
Motoyama, H., Enomoto, H., Furukawa, T., Kamiyama, K., Shoji, H., Shiraiwa, T., Watanabe, K., Namasu, K., and Ikeda, H.: Preliminary study of ice flow observations along traverse routes from coast to Dome Fuji, East Antarctica by differential GPS method., Nankyoku Shiryo (Antarctic Record), 39, 94–98, 1995. 2072
Matsuoka, K., Maeno, H., Uratsuka, S., Fujita, S., Furukawa, T., and Watanabe, O.: A ground-based, multi-frequency ice-penetrating radar system, Ann. Glaciol., 34, 171–176, doi:10.3189/172756402781817400, 2002. 2071
Moore, J. C., Mulvaney, R., and Paren, J. G.: Dielectric stratigraphy of ice: a new technique for determining total ionic concentrations in polar ice, Geophys. Res. Lett., 16(10), 1177–1180, doi:10.1029/GL016i010p01177, 1989. 2068
Mosley-Thompson, E., Paskievitch, J. F., Gow, A. J., and Thompson, L. G.: Late 20th century increase in South Pole snow accumulation, J. Geophys. Res., 104(D4), 3877–3886, doi:10.1029/1998JD200092, 1999. 2064, 2086
Oerter, H., Wilhelms, F., Jung-Rothenhäusler, F., Göktas, F., Miller, H., Graf, W., and Sommer, S.: Accumulation rates in Dronning Maud Land, Antarctica, as revealed

TCD
5, 2061–2114, 2011

by dielectric-profiling measurements of shallow firn cores Ann. Glaciol., 30(1), 27–34, doi:10.3189/172756400781820705, 2000. 2086
Parrenin, F., Dreyfus, G., Durand, G., Fujita, S., Gagliardini, O., Gillet, F., Jouzel, J., Kawamura, K., Lhomme, N., Masson-Delmotte, V., Ritz, C., Schwander, J., Shoji, H., Uemura, R., Watanabe, O., and Yoshida, N.: 1-D-ice flow modelling at EPICA Dome C and Dome Fuji, East Antarctica, Clim. Past, 3, 243–259, doi:10.5194/cp-3-243-2007, 2007. 2072, 2073
Pruett, L. E., Kreutz, K. J., Wadleigh, M., Mayewski, P. A., and Kurbatov, A.: Sulfur isotopic measurements from a West Antarctic ice core: implications for sulphate source and transport, Ann. Glaciol., 39(1), 161–168, doi:10.3189/172756404781814339, 2004. 2067
Reijmer, C. and Van den Broeke, M. R.: Temporal and spatial variability of the surface mass balance in Dronning Maud Land, Antarctica, as derived from automatic weather stations, J. Glaciol., 49(167), 512–520, doi:10.3189/172756503781830494, 2003. 2074, 2103, 2109
Richardson, C., Aarholt, E., Hamran, S.-E., Holmlund, P., and Isaksson, E.: Spatial distribution of snow in western Dronning Maud Land, East Antarctica, mapped by a ground-based snow radar, J. Geophys. Res., 102(B9), 20343–20353, doi:10.1029/97JB01441, 1997. 2070
Rotschky, G., Eisen, O., Wilhelms, F., Nixdorf, U., and Oerter, H.: Spatial distribution of surface mass balance on Amundsenisen plateau, Antarctica, derived from ice-penetrating radar studies, Ann. Glaciol., 39, 265–270, doi:10.3189/172756404781814618, 2004. 2080
Rotschky, G., Holmlund, P., Isaksson, E., Mulvaney, R., Oerter, H., Van den Broecke, M. R., and Winther, J.-G.: A new surface accumulation map for western Dronning Maud Land, Antarctica, from interpretation of point measurements, J. Glaciol., 53(182), 385–398, doi:10.3189/002214307783258459, 2007. 2071, 2080
Ruth, U., Barnola, J.-M., Beer, J., Bigler, M., Blunier, T., Castellano, E., Fischer, H., Fundel, F., Huybrechts, P., Kaufmann, P., Kipfstuhl, S., Lambrecht, A., Morganti, A., Oerter, H., Parrenin, F., Rybak, O., Severi, M., Udisti, R., Wilhelms, F., and Wolff, E.: "EDML1": a chronology for the EPICA deep ice core from Dronning Maud Land, Antarctica, over the last 150 000 years, Clim. Past, 3, 475–484, doi:10.5194/cp-3-475-2007, 2007. 2070, 2072
Stenni, B., Proposito, M., Gragnani, R., Flora, O., Jouzel, J., Falourd, S., and Frezzotti, M.: Eight centuries of volcanic signal and climate change at Talos Dome (East Antarctica), J. Geophys. Res., 107(D9), 4076, doi:10.1029/2000JD000317, 2002. 2087
Surdyk, S.: Using microwave brightness temperature to detect short-term surface air temperature changes in Antarctica: An analytical approach, Remote Sens. Environ., 80(2), 256–271, doi:10.1016/S0034-4257(01)00308-X, 2002. 2082

TCD
5, 2061–2114, 2011

Surdyk, S. and Fily, M.: Comparison of the passive microwave spectral signature of the Antarctic ice sheet with ground traverse data, Ann. Glaciol., 17, 161–166, 1993. 2081, 2082, 2114
Surdyk, S. and Fily, M.: Results of a stratified snow emissivity model based on the wave approach: Application to the Antarctic Ice Sheet, J. Geophys. Res., 100(C5), 8837–8848, doi:10.1029/94JC03361, 1995. 2082, 2114
Takahashi, S., Kameda, T., Enomoto, H., Motoyama, H., and Watanabe, O.: Automatic Weather Station (AWS) data collected by the 33rd to 42nd Japanese Antarctic Research Expeditions during 1993–2001 in JARE data reports, Meteorology, National Institute of Polar Research, Tokyo, 416 pp., 2004. 2074, 2103, 2110
Traufetter, F., Oerter, H., Fischer, H., Weller, R., and Miller, H.: Spatio-temporal variability in volcanic sulphate deposition over the past 2 kyr in snow pits and firn cores from Amundsenisen, Dronning Maud Land, Antarctica, J. Glaciol., 50(168), 137–146, doi:10.3189/172756504781830222, 2004 2067
Trepte, C. R., Veiga, R. D., and McCormick, M. P.: The poleward dispersal of Mount Pinatubo volcanic aerosol, J. Geophys. Res., 98(D10), 18563–18573, doi:10.1029/93JD01362, 1993. 2067
Urbini, S., Frezzotti, M., Gandolfi, S., Vincent, C., Scarchilli, C., Vittuari, V., and Fily, M.: Historical behaviour of Dome C and Talos Dome (East Antarctica) as investigated by snow accumulation and ice velocity measurements, Global Planet. Change, 60, 576–588, doi:10.1016/j.gloplacha.2007.08.002, 2008. 2087
Van de Berg, W., Van den Broeke, M., Reijmer, C., and Van Meijgaard, E.: Reassessment of the Antarctic surface mass balance using calibrated output of a regional atmospheric climate model, J. Geophys. Res., 111, D11104, doi:10.1029/2005JD006495, 2006. 2063
Van As, M. R., Van den Broeke, M. R., and Helsen, M.: Strong-wind events and their impact on the near-surface climate at Kohnen Station on the Antarctic Plateau, Antarct. Sci., 19(4), 507–519, doi:10.1017/S095410200700065X, 2007. 2078
Van den Broeke, M. R. and Van Lipzig, N. P. M.: Factors controlling the near-surface wind field in Antarctica, Mon. Weather Rev., 131, 733–743, doi:10.1175/1520-0493(2003)131<0733:FCTNSW>2.0.CO;2, 2003. 2077
Van Lipzig, N. P. M., Turner, J., Colwell, S. R., and Van den Broeke, M. R.: The near-surface wind field over the Antarctic continent, Int. J. Climatol., 24, 1973–1982, doi:10.1002/joc.1090, 2004. 2077
Vaughan, D., Bamber, J., Giovinetto, M., Russell, J., and Cooper, A.: Reassessment of

TCD
5, 2061–2114, 2011

net surface mass balance in Antarctica, J. Climate, 45(150), 933–946, doi:10.1175/1520-0442(1999)012<0933:RONSMB>2.0.CO;2, 1999. 2064
Velicogna, I. and Wahr, J.: Measurements of time-variable gravity show mass loss in Antarctica, Science, 311, 1754–1756, doi:10.1126/science.1123785, 2006. 2063
Ulaby, F. T., Moore, R. K., and Fung, A. K.: Microwave Remote Sensing: Active and Passive, Addison-Wesley Publishing Co., 925–966, 1982. 2085
Watanabe, O.: Distributions of surface features of snow cover in Mizuho Plateau., Mem. Natl Inst. Polar Res. Spec. Issue., 7, 44–62, 1978. 2077, 2078
Watanabe, O., Fujii, Y., Motoyama, H., Furukawa, T., Shoji, H., Enomoto, H., Kameda, T., Narita, H., Naruse, R., Hondoh, T., Fujita, S., Mae, S., Azuma, N., Kobayashi, S., Nakawo, M., and Ageta, Y.: Preliminary study of ice core chronology at Dome Fuji, Proc. NIPR Symp. Polar Meteorol. Glaciol., 11, 9–13, 1997. 2069
Watanabe, O., Jouzel, J., Johnsen, S., Parrenin, F., Shoji, H., and Yoshida, N.: Homogeneous climate variability across East Antarctica over the past three glacial cycles, Nature, 422, 509–512, doi:10.1038/nature01525, 2003. 2100
Wilhelms, F.: Explaining the dielectric properties of firn as a density-and-conductivity mixed permittivity (DECOMP), Geophys. Res. Lett., 32(16), L16501, doi:10.1029/2005GL022808, 2005. 2068
Wilhelms, F., Kipfstuhl, J., Miller, H., Heinloth, K., and Firestone, J.: Precise dielectric profiling of ice cores: a new device with improved guarding and its theory, J. Glaciol., 44(146), 171–174, 1998. 2068
Wolff, E. W.: Electrical stratigraphy of polar ice cores: principles, methods, and findings, in: Physics of Ice Core Records, edited by: Hondoh, T., Hokkaido University Press, Sapporo, 155–171, 2000. 2068

TCD
5, 2061–2114, 2011

Table 1. Major sites along the JASE traverse and related sites.

Site name	Lat. ° S	Long. ° [a]	Elevation(m)	*H* (m)[b]	Note
S16	69.030	40.052	589	350	Base of the Japanese team near the coast.
Mizuho	70.697	44.274	2250	2060	
MD364	74.008	42.996	3347	2716	Mid-point between Mizuho and Dome Fuji
MD550	75.676	41.539	3663	2472	
DF	77.317	39.703	3800	3028	Dome Fuji Station: deep ice coring site (Watanabe et al., 2003)
DK190	76.794	31.900	3741	2919	Science stop for installing an automatic weather station
MP	75.888	25.834	3661	2820	Meeting point of the two teams. AWS JASE2007 was installed.
A38	75.287	18.421	3543	2706	Junction of the Swedish inbound and return trips
A28	74.862	14.742	3466	–	Junction of the Swedish inbound and return trips
RT459	77.376	37.932	3780	3333	Subglacial Lake Point
RT313	77.961	32.624	3620	3550	Southernmost point of the JASE traverse.
RT188	77.161	29.426	3678	2574	
RT155	76.869	29.270	3701	2702	
RT103	76.762	27.248	3653	3019	
A35	76.066	22.459	3586	–	One of the junctions between the JASE traverse and the Norway-US traverse
A37	75.654	19.240	3544	–	Same as above
FB0603	75.117	9.724	3300	–	Firn coring site by the Alfred Wegener Institute, Germany in 2006
A23	75.168	6.493	3174	–	Junction of the Swedish inbound and outbound trips
FB0601	75.247	4.844	3090	–	Firn coring site by the Alfred Wegener Institute, Germany in 2006
EPICA DML	75.002	0.068	2890	2774	2774-m long ice coring site (EPICA Community Members, 2006)
Wasa Station	73.053	–13.374	292	383	Base of the Swedish team
Svea Station	74.571	–11.170	1313	715	Swedish station
IPY Site1	75.001	–10.121	2528	1603	Science site
Site M	75.000	15.000	3457	–	Science sites in Hofstde et al. (2004) and Isaksson et al. (1996)
Site L	74.647	12.790	3420	–	Junction with the Norway-US traverse
NUS07-3	77.000	26.050	3582	–	Science sites in Anschütz et al. (2009) and Müller et al. (2010)
NUS07-4	78.217	32.850	3595	–	Same as above
Plateau Station	79.250	40.500	3634	–	Koerner (1971)

[a] Positive and negative longitude number mean East and West, respectively.
[b] *H*: ice thickness (m).

TCD
5, 2061–2114, 2011

Table 2a. Annual accumulation rates derived for Dome Fuji, DK190 and MP.

Period (AD)	Time span	Site name			Data source	Error
		Dome Fuji	DK190	MP		
1993–2008	15	25.6 ± 1.7 ($kg\,m^{-2}\,a^{-1}$)	34.1 ± 2.3	41.9 ± 2.8	Pit studies (JASE 2007/08)[a]	b
1995–2006	11	27.3 ± 0.4	–	–	Snow stake farm (Kameda et al., 2008)	c
1994–2001	7	29.5 ± 4.2	–	–	Analysis of firn core (Igarashi et al., 2011)	b
1964–2008	44	28.8 ± 0.7	–	38.7 ± 0.9	Firn core and pit studies (JASE 2007/08)	b
1286–2008	722	24.5 ± 0.7	28. 7 ± 0.9	33.1 ± 1.0	Ground Penetrating Radar (JASE 2007/08)	d
1260–2001	741	25.5 ± 0.3	–	–	Analysis of firn core (Igarashi et al., 2011)	e
–2008	7.9 ± 0.5k	25.0 ± 1.3	28.7 ± 1.5	33.9 ± 1.7	Radar (JASE 2007/08) and Dome Fuji core	d

[a] Pit is located at 77.298° S and 39.786° E, and is ~3 km from the Dome Fuji Station.
[b] Error range was assumed to be equivalent to 1 yr accumulation, with a confidence level of ~83 %.
[c] Error is the standard deviation of the mean, with a confidence level of ~68 %.
[d] Major source of error was assumed to be caused by 3 % of the density estimation within firn.
[e] Major source of error was assumed to be caused by 1 % of the density estimation within firn.

TCD
5, 2061–2114, 2011

Table 2b. Annual accumulation rates derived form firn core studies at sites between A35 and EPICA DML

Period(AD)	Time span	Site name					Data source	Error
		A35	A28	FB0603	FB0601	EPICA DML		
1964–2008	44	39.2 ± 0.9	44.5 ± 1.0	38.0 ± 0.9	51.6 ± 1.2	73.1 ± 1.7	Firn cores (JASE 2007/08, AWI 2003/04 and 2005/06)	b

TCD
5, 2061–2114, 2011

Table 3. Comparison between orientation of surface snow features and windfield

Site	Orientation of surface snow features (this work)[a]	Average direction of wind vector calculated from meteorological data	Wind direction for strong-wind events	Station ID of AWS or data source	Year of the observational data	Reference
EPICA DML	45°(this work)	57°[b]	45°	Utrecht University/ IMAU AWS9	1998–2000, 2002–05	Birnbaum et al. (2010), Reijmer and Van den Broeke (2003)
MP	70°	82°	70 ±24°[c]	ARGOS AWS No. 30305 (JASE2007)	2009	Keller et al. (2010)
Dome Fuji	50°	100°	53 ±48°[d]	CMOS AWS at Dome Fuji Station	1994–2001	Takahashi et al. (2004)
MD364	102°	119°	120 ±22°[e]	ARGOS AWS No. 8198	2002	Keller et al. (2010)

[a] Mean value in the vicinity of each site, with errors of ±10°.
[b] Value at EPICA DML is cited from Birnbaum et al. (2010).
[c] An average wind direction for wind speeds above 10 m s^{-1} observed in ~6 % of cases.
[d] An average wind direction for wind speeds above 8 m s^{-1} observed in ~1 % of cases.
[e] An average wind direction for wind speeds above 10 m s^{-1} observed in ~14 % of cases.

TCD
5, 2061–2114, 2011

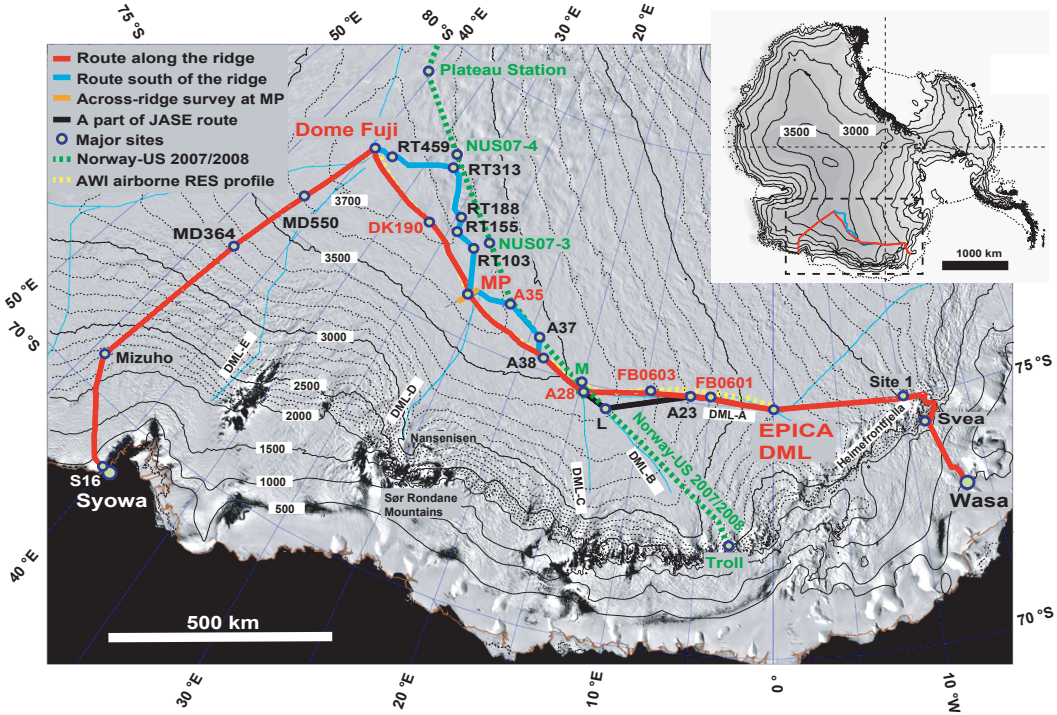

Fig. 1. Routes of the JASE traverse shown on a map of Antarctica. Surface elevation contour curves have spacing of 500 m below 2000 m and of 100 m above 2000 m. The satellite image is the MODIS mosaic of Antarctica (Haran et al., 2005). The red trace shows the route between S16 and Wasa. The blue trace shows the south routes (see text). Major sites are indicated by circular symbols (see also Table 1). Sites for pit studies and firn core studies are shown in red letters. The orange line at MP is the trace of the cross-ridge survey (see text). The black thick trace is also a part of the JASE traverse. The green dotted trace is the route of the Norway-US traverse in the same 2007/2008 season (Anschütz et al., 2009). Site names related to it are shown with green letters. The yellow dashed trace is the route of an earlier airborne radar sounding (Huybrechts et al., 2009). Light blue thin traces indicate ridges on the ice sheet surface. For convenience, we labelled the ridges DML-A to DML-E.

TCD
5, 2061–2114, 2011

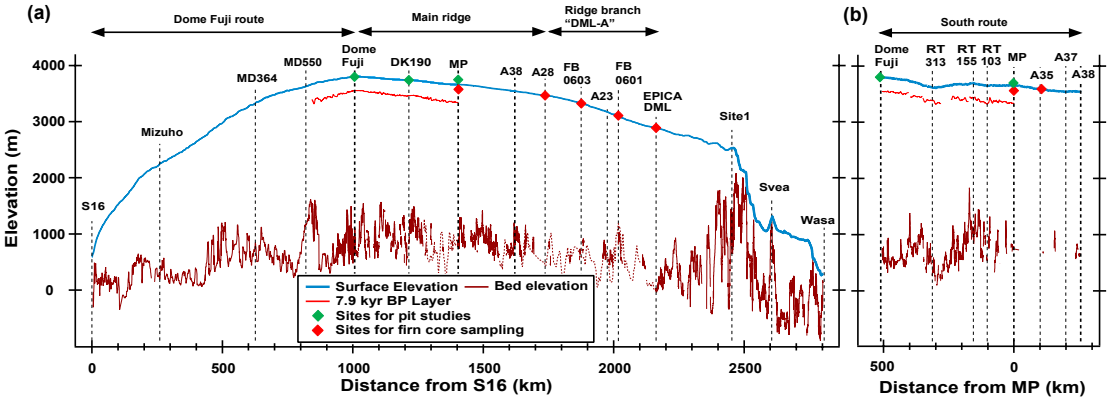

Fig. 2. Cross section of the ice sheet along the JASE traverse. **(a)** The main ridge route is indicated as a red trace in Fig. 1. **(b)** The south routes are indicated as blue traces in Fig. 1. Abscissas show **(a)** distance along the traverse from S16 toward Wasa Station and **(b)** distance from MP along the south routes. The vertical exaggeration is 200 times. Vertical dashed lines show the location of major sites. Surface elevation data (blue curves) are based on the digital elevation model (Bamber et al., 2006). A shallow isochrone within the ice sheet is indicated as a red profile based on analysis of the radar sounding data. It is dated as a 7.9 ± 0.5 kyr BP layer (see text). Bed elevation was derived from the radar sounding data. For some locations where the bed signal was undetected in the JASE traverse, ice thickness data from an earlier airborne radar sounding (Huybrechts et al., 2009), is shown as a thin dotted profile. Sites with symbols indicate sites of pit studies and/or firn core sampling (see text).

TCD
5, 2061–2114, 2011

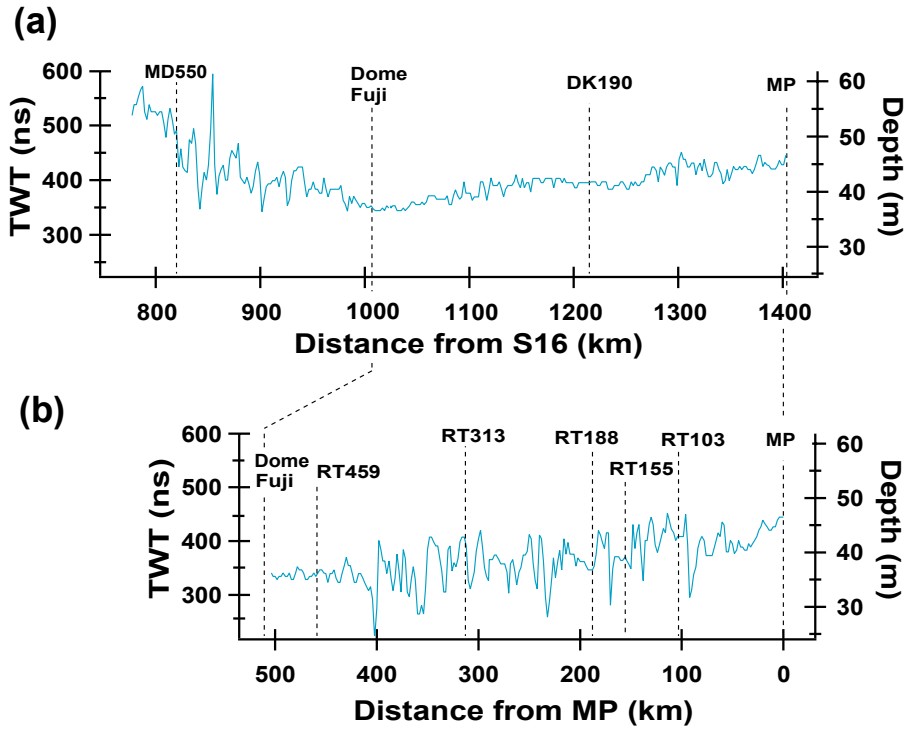

Fig. 3. Results of ground penetrating radar (GPR) measurements. The figure shows the two-way travel time (TWT) of radio waves to an isochronous layer along the traverse routes. The corresponding depth scale is shown on the right axis. Upper graph labelled **(a)** shows data along the ridge route. Lower graph labelled **(b)** shows data along the south route. Features of the data are discussed in the text.

TCD
5, 2061–2114, 2011

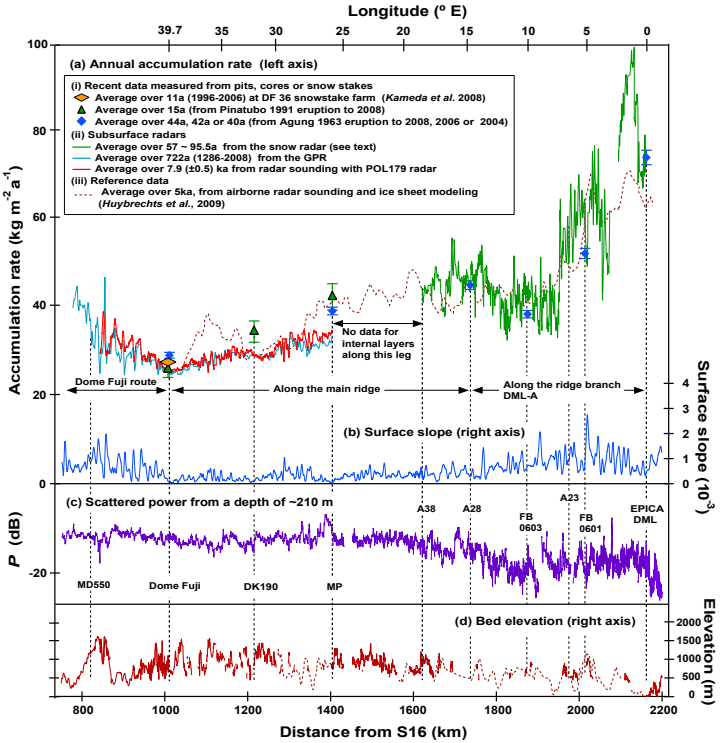

Fig. 4. Annual accumulation rate over various time scales are shown with indicators of the depositional environment, along the main route of the traverse. The abscissa represents distance from S16 along the traverse route. Details are as follows. **(a)** Annual accumulation rate averaged over various time scales. Pit studies and firn core studies provided accumulation rates averaged over 44 yr and/or 15 yr (see text). Also shown is the annual accumulation rate averaged over 11 yr from 1996 to 2006 (Kameda et al., 2008) from a stake farm with 36 stakes at Dome Fuji. Subsurface radars provide annual accumulation rates averaged over 57–96 yr, ~722 yr and 7.9 k yr. Details are given in the text. Brown dashed line shows earlier data for comparison; annual accumulation rate averaged over 5 ka derived from isochrones of airborne radar sounding data and 3-D modelling of the ice sheet (Huybrechts et al., 2009). **(b)** Surface slope at each point along the route was calculated using the digital elevation model of Bamber et al. (2006). **(c)** Relative variation (in dB) of the received power for 179-MHz radio waves from within the ice sheet at a depth of ~210 m (see text). **(d)** Bed elevation derived from radar sounding.

TCD
5, 2061–2114, 2011

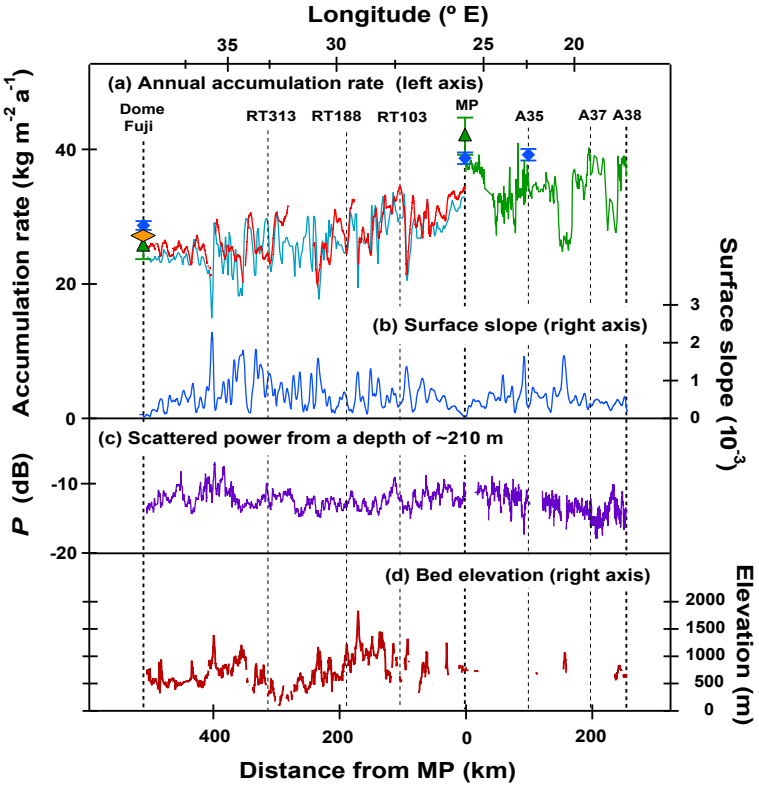

Fig. 5. Annual accumulation rate over various time scales are shown with indicators of the depositional environment, along the south route. Again, surface slopes, normal backscattered strength of radio waves from a shallow depth range, and bed elevation are shown as in Fig. 4. The abscissa indicates distance from MP along the traverse route. All other items and symbols are the same as in Fig. 4. Fluctuations of the accumulation rate, surface slope and backscattered strength of radio waves are much larger than those along the route in Fig. 4.

TCD
5, 2061–2114, 2011

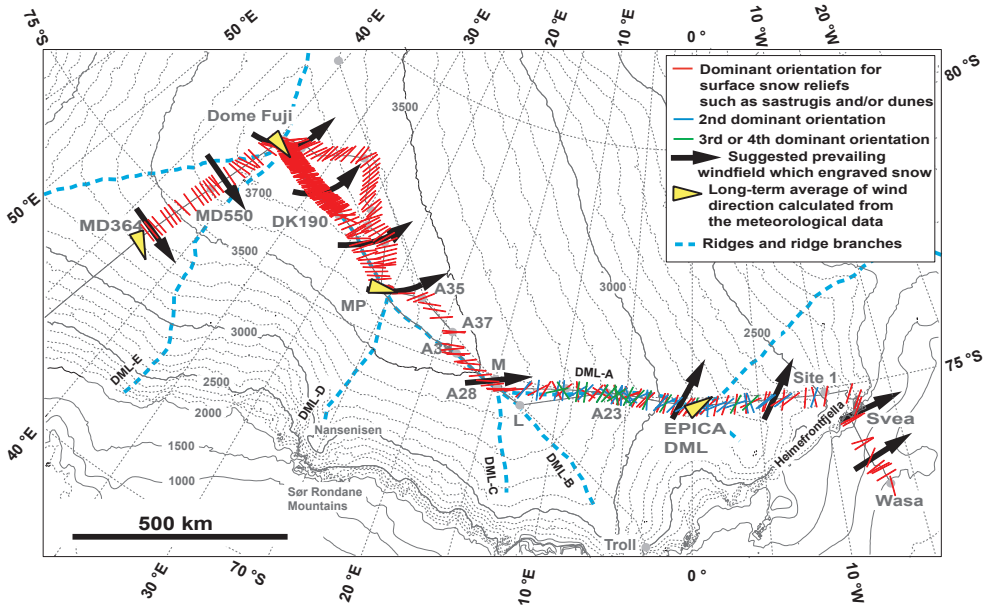

Fig. 6. Dominant orientation of surface snow reliefs such as sastrugis and dunes were observed along the traverse routes between MD364 and Wasa. Orientations are plotted as thin lines on the map. At some sites, two or more orientations were observed, in particular at sites between A28 and A23. The most dominant orientations are shown as red symbol marker. The second and higher ones are shown as green and blue markers, respectively. Arrows with the thick black lines/curves are the suggested direction of strong winds ($>\sim 10\,m\,s^{-1}$) that caused the surface snow reliefs. Yellow arrows represent orientation of the average windfield at MD364, DF, MP and EPICA DML. For MD364, DF and MP, the yellow arrows show the directions of average wind vectors. Details are given in Table 3. At EPICA DML, the yellow arrow represents the long-term average wind direction (Birnbaum et al., 2010; Reijmer and Van den Broeke, 2003). Bold blue dashed curves indicate ridges on the ice sheet surface.

TCD
5, 2061–2114, 2011

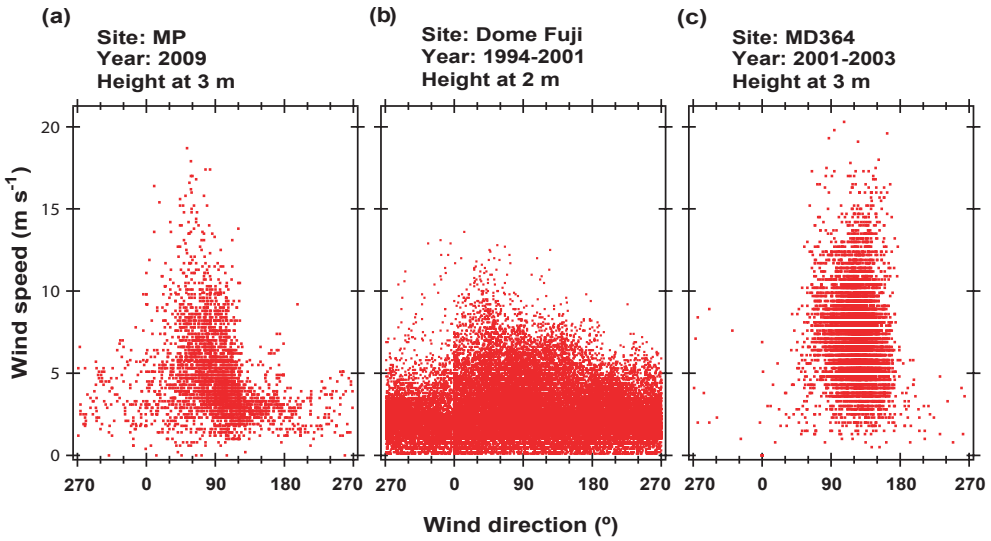

Fig. 7. Relationship between wind speed and direction at the three AWS sites along the JASE traverse. **(a)** Data at MP during the year 2009. The observation data is from the AWS JASE2007. Data selected at three hourly intervals were used. Of the measured events, 6 % have wind speeds of than 10 m s^{-1}, with an average wind direction of 70° (±24°, standard deviation). **(b)** Data at Dome Fuji during the years from 1994 to 2001 (Takahashi et al., 2004). Data with hourly intervals were used. Of the measured events, 1 % has wind speeds of than 8 m s^{-1}, with an average wind direction of 53° (±48°). **(c)** Data at MD364 during the years from 2001 to 2003 (Keller et al., 2010). Data with three hourly intervals were used. Of the measured events, 14 % has wind speeds of than 10 m s^{-1}, with an average wind direction of 120° (±22°).

TCD
5, 2061–2114, 2011

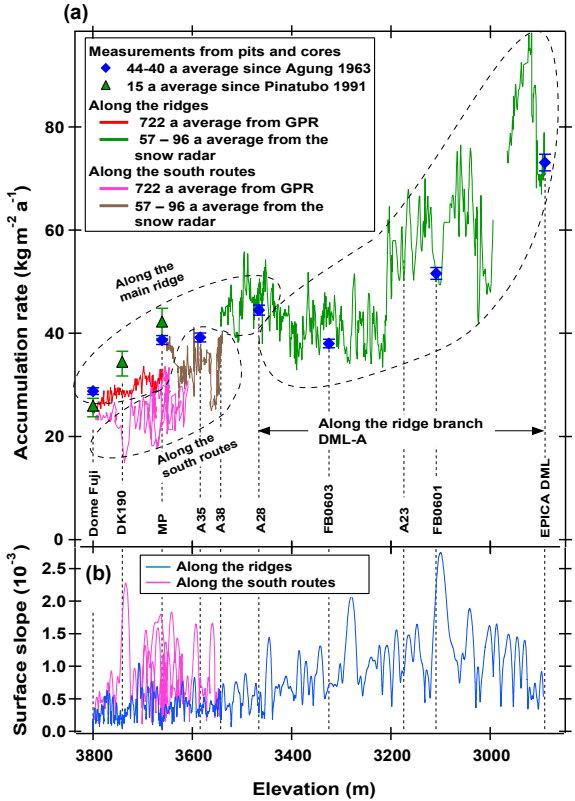

Fig. 8. Values of accumulation rate are shown versus site elevation. Panel **(a)** shows data selected from Figs. 4a and 5a. The group in the upper left is data from sites along the main ridge between Dome Fuji and A28. The group at the lower left side is data from sites along the south route between Dome Fuji and A38. The group on the right side is data from sites along the ridge branch DML-A between A28 and EPICA DML. Panel **(b)** shows surface slope.

TCD
5, 2061–2114, 2011

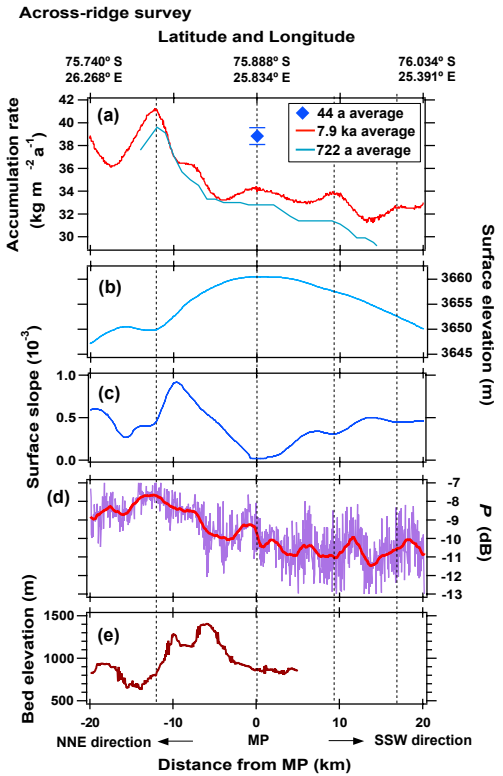

Fig. 9. Annual accumulation rate for the 40-km-long cross-ridge survey at MP. **(a)** Annual accumulation rates averaged over 7.9 ka (red trace) and 722 a (blue trace) are determined from data of subsurface radars. They are compared with the average over 44 a at MP. Also shown are **(b)** surface elevation, **(c)** surface slope, **(d)** normal backscattered strength of radio waves from a depth of 210 m, and **(e)** bed elevation. An accumulation rate decrease from the northern coastal side of the ridge toward the southern interior side. Annual accumulation rate is locally higher at locations with flat or concave surface topography, as indicated by thin vertical dashed lines. Similarly, the annual accumulation rate is locally lower at locations with steep surfaces or a convex surface topography. The normal backscattered strength also decreases toward interior of the ice sheet.

TCD
5, 2061–2114, 2011

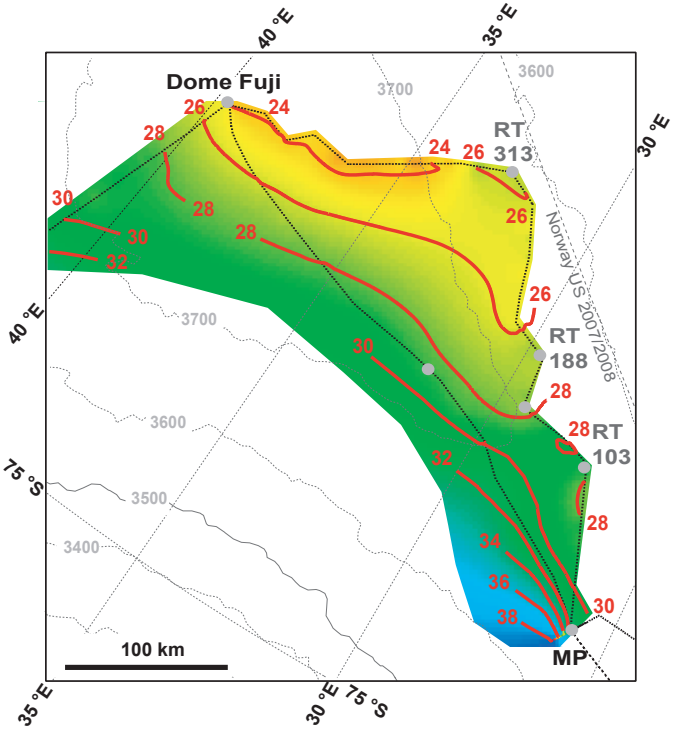

Fig. 10. Map of annual accumulation rate averaged over 722 a, derived from the GPR data. Colour scale image with bold red contours and red letters shows the distribution of the accumulation rate in kg m^{-2} a^{-1}. Surface elevation of the ice sheet is also shown by thin gray contour curves. The purpose of this map is to visualize the large-scale spatial distribution of the accumulation rate in this area. For this purpose, the original data was smoothed over a distance of 40 km to reduce fluctuations.

TCD
5, 2061–2114, 2011

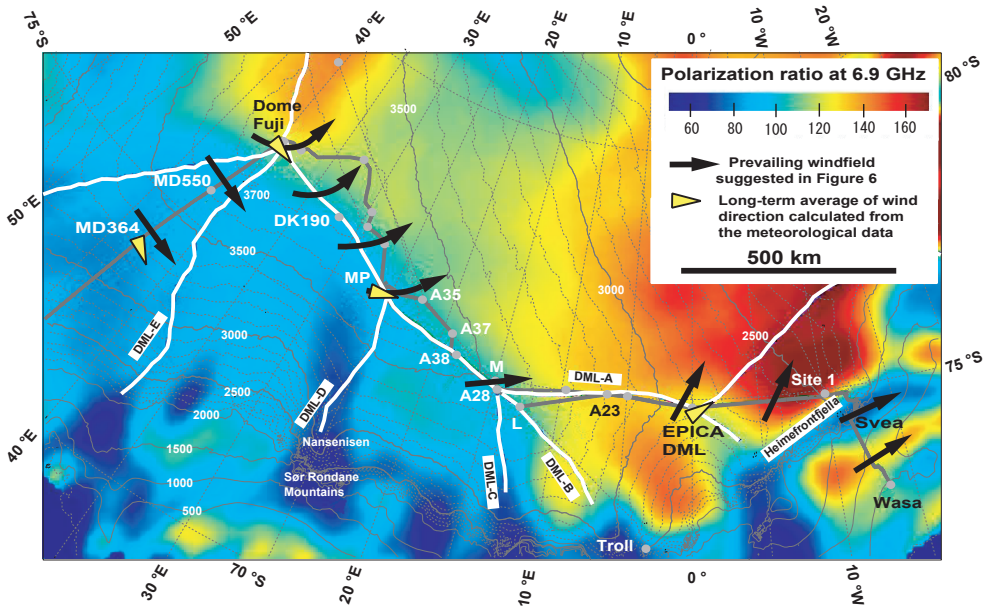

Fig. 11. Distribution of the polarization ratio of the passive microwave data at 6.9 GHz. Data were obtained from the Advanced Microwave Scanning Radiometer for EOS (AMSR-E), which was developed by JAXA for use on board the EOS satellite that has been operating since 2002. Previous studies (Surdyk and Fily, 1993, 1995) suggested that the polarization ratio at frequencies lower than 10 GHz is an indicator of the number of layers per unit depth of strata to a depth of ~2 m. Lower/higher values mean fewer/more layers in the strata, which would qualitatively suggest that the accumulation rate is higher/lower. In the area between Dome Fuji and MP, the distribution of the polarization ratio closely resembles that of the accumulation rate shown in Fig. 10. The ridge branch DML-A between site A28 and EPICA DML is within an area of higher polarization ratio. In addition, the leg between Troll Station and site M is also within an area of higher polarization ratio.

TCD
5, 2061–2114, 2011